JOURNAL OF GEOPHYSICAL RESEARCH, VOL. 105, NO. B3, PAGES 5859–5885, MARCH 10, 2000

Deep structure of the ocean-continent transition in the southern Iberia Abyssal Plain from seismic refraction profiles: The IAM-9 transect at 40°20'N

S. M. Dean[1] and T. A. Minshull[1]
Bullard Laboratories, Department of Earth Sciences, University of Cambridge, Cambridge, England, U.K.

R. B. Whitmarsh
Challenger Division, Southampton Oceanography Centre, Southampton, England, U.K.

K. E. Louden
Department of Oceanography, Dalhousie University, Halifax, Nova Scotia, Canada

Abstract. We present a crust and mantle velocity structure for the West Iberia passive continental margin derived from a 320-km-long wide-angle seismic profile acquired in the southern Iberia Abyssal Plain. We observe a 170-km-wide ocean-continent transition zone which includes a pair of overlapping peridotite ridges and is bounded by oceanic crust and landward by fault-bounded blocks of continental crust. The profile lies ~40 km south of the transect sampled by Ocean Drilling Program (ODP) Legs 149 and 173. The transition zone structure can be divided into an upper layer, 2–4 km thick with velocities of between 4.5 and 7.0 km s^{-1} and generally a high-velocity-gradient (1 s^{-1}), and a lower layer up to 4 km thick with a velocity of ~7.6 km s^{-1} and a low-velocity-gradient. A weak Moho reflection in this zone was seen only on wide-angle profiles at an offset of ~30 km. The upper layer has a distinctly lower velocity than thinned continental crust adjacent to the continental slope. Conversely, the lower layer has too high a velocity to be magmatically intruded or underplated lower continental crust. On the coincident seismic reflection profile, fault-bounded crustal blocks, identified in unequivocal extended continental crust, are not observed in the transition zone. The upper layer has velocity bounds and gradient similar to oceanic layer 2 observed west of the peridotite ridges, but no oceanic layer 3 velocity structure is present. While magnetic anomalies have been identified within the transition zone, they have not been modeled successfully as seafloor spreading magnetic anomalies, nor do they generally form long linear margin-parallel features. Finally, ODP boreholes, ~40 km north of our profile and within the interpreted transition zone, have recovered up to 140-m-thick sections of serpentinite and serpentinized peridotites with little evidence of mafic igneous material. We conclude that the transition zone cannot be dominantly composed of either extended continental crust or oceanic crust. Although current melting models predict a considerably thicker crust of decompression melt products, we interpret this region as exposed upper mantle peridotite with little or no synrift extrusive material and limited amounts of synrift material intruded within the serpentinized peridotite.

1. Introduction

The study of the structure and composition of passive continental margins provides an insight into the mechanisms of continental rifting and its evolution to seafloor spreading. Continental rifting involves a combination of tectonic and magmatic processes. Tectonic models have broadly concentrated on the relative contributions of pure and/or simple shear in the lithosphere. Magmatism during rifting is principally dependent on mantle temperature, rate and duration of extension, and the initial lithospheric thickness [*Bown and White*, 1995]. Continental margins have been divided into one of two types depending on the apparent

[1]Now at School of Ocean and Earth Sciences, Southampton Oceanography Centre, Southampton, England, United Kingdom.

Paper number 1999JB900301.
0148-0227/00/1999JB900301$09.00

Table 1. Widths of Extended Continental Crust and "Transition Zone" for Nonvolcanic Rifted Margins in the North Atlantic and Labrador Sea Region

Nonvolcanic Rifted Margin	Width of Extended Continental Crust, km	Width of Transition Zone Crust, km	Total Width, km
South West Greenland[a]	70	75	145
Southern Labrador[b]	140	75	215
Southern Flemish Cap[c]	50	>120	>170
Newfoundland (44°N)[d]	~70	>90	>160
Goban Spur[e]	80	?	80?
Northern Bay of Biscay[f]	~180	?	180?
Galicia Bank[g]	~100	<10	110
Southern IAP (ODP profile)	~150[h]	>40[i]	>190
Southern IAP (IAM-9 profile)[j]	~60	170	220
Tagus Abyssal Plain[k,l]	100–150	50–80	150–230

See Figure 1. Widths are reinterpreted using the following definitions. "Transition zone" is defined seismically by a thin (<3 km) upper layer with velocity <7.0 km s^{-1}, and a high-velocity lower layer (or low-velocity upper mantle) with velocity between 7.0 and 7.9 km s^{-1}. The landward limit of extended continental crust is defined with wide-angle seismic data as the point at which the Moho first flattens to give a maximum crustal thickness (in all cases >20 km) or with seismic reflection profiles as the point at which acoustic basement stops shallowing landward of any faulted basement blocks. This definition includes only continental crust extended during the stage of rifting which immediately preceded seafloor spreading. Question marks indicate where the width of the "transition zone" is unconstrained.

[a] *Chian and Louden* [1994].

[b] *Chian et al.* [1995].

[c] *Todd and Reid* [1989]; we interpret lines HU-1 and HU-2 to lie over transitional crust.

[d] *Reid* [1994]; we identify no oceanic velocity structure.

[e] *Horsefield et al.* [1993]; we do not identify any transitional crust but all instruments lie over thinned continental crust.

[f] *Le Pichon and Barbier* [1987].

[g] *Whitmarsh et al.* [1996].

[h] *Beslier et al.* [1993].

[i] *Chian et al.* [1999].

[j] *Pickup et al.* [1996]; transition zone width is 130 km not including the two overlapping segments of peridotite ridge.

[k] *Pinheiro et al.* [1992].

[l] *Mauffret et al.* [1989].

degree of rift-related magmatism. A margin is determined to have a "volcanic" character if a seaward dipping reflector sequence, the expression of subaerial lava flows [*Eldholm et al.*, 1987], and/or a several kilometer thick high-velocity (~7.2 km s^{-1}) layer at the base of the crust, representing underplated material, is observed [*Mutter*, 1993]. A "nonvolcanic" margin lacks these features; instead, fault-bounded basement blocks are identified. Nonvolcanic margins in the North Atlantic region are characterized by the lack of a distinct boundary between thinned continental crust and normal Atlantic oceanic crust; rather there exists a transition from one crustal type to the other (Table 1 and Figure 1).

The "transition zone" has a distinct velocity structure. In almost every case, the transition zone has a thin upper layer <3 km thick with velocities between 4.0 and 6.5 km s^{-1} and a high-velocity-gradient and has a high-velocity lower layer with velocity of around 7.6 km s^{-1} and a low-velocity-gradient. The Moho is also absent or weak. Off the West Iberia margin (Galicia Bank and the southern Iberia Abyssal Plain (IAP)), the transition zone includes a peridotite ridge (or, as is the case off Galicia Bank, the transition zone is a peridotite ridge), with velocity ~6.5–7.5 km s^{-1}. The width of extended continental crust and the transition zone is variable (Table 1), but in general, where the transition zone is wide, the region of extended continental crust is relatively narrow (e.g., Southern Flemish Cap and the IAM-9 profile in the southern IAP), and where the region of extended continental crust is wide, the transition zone is relatively narrow (e.g., Labrador Sea, Northern Bay of Biscay, Galicia Bank, the Ocean Drilling Program (ODP) Leg 149/173 drilling profile in the southern IAP and in the Tagus Abyssal Plain). Typically, the sum of extended continental crust and transition zone is 100–200 km in the North Atlantic.

The West Iberia margin in the eastern North Atlantic is perhaps one of the best studied of the continental margins. It is particularly suited for investigation since

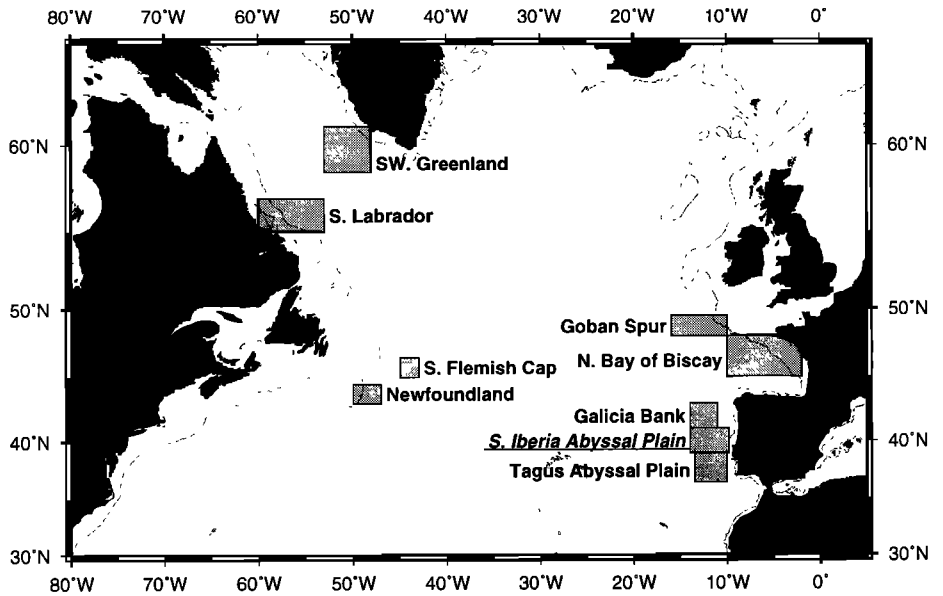

Figure 1. North Atlantic and Labrador Sea region; the southern Iberia Abyssal Plain is located at approximately 40°N, 12°W on the West Iberia Atlantic margin. The 500-m bathymetric contour (dotted line) marks the approximate extent of the continental shelf. Shaded boxes locate seismic surveys on margins interpreted to be nonvolcanic in character by various authors (Table 1).

it has been relatively starved of sediment. It is characterized by distinct bathymetric regions. From north to south we observe Galicia Bank, a region of relatively shallow and rough seafloor topography, the southern IAP, the narrow Estremadura Spur, and the Tagus Abyssal Plain (Figure 2). No seaward dipping reflector sequences have been recognized anywhere on this margin. Significant quantities of possibly synrift magmatic material have only been recovered by offshore drilling at one location (Site 900 [*Sawyer et al.*, 1994]), and no significant quantities have been observed onshore [*Pinheiro et al.*, 1996]. This margin is therefore termed a nonvolcanic continental margin. However, this classification does not exclude the possibility that there was some minor rift-related magmatism on this margin, and this point will form part of our later discussion.

Modeling of magnetic anomalies in the southern IAP [*Whitmarsh et al.*, 1990, 1996; *Whitmarsh and Miles*, 1995] successfully fits anomaly M3 as the earliest isochron formed by seafloor spreading. The modeling was constrained by the prominent J magnetic anomaly which is observed along the central and southern North Atlantic margins and is associated with M0 on the West Iberia margin [*Rabinowitz et al.*, 1979].

Numerous seismic reflection profiles along the margin exhibit a basement high which has been identified as a peridotite ridge (PR), so named after sampling where it locally outcrops west of Galicia Bank [*Boillot et al.*, 1980]. Four segments of the peridotite ridge have been identified from Galicia Bank to the southern IAP on existing profiles [*Beslier et al.*, 1993]. It appears to coincide with the eastward boundary of seafloor spreading magnetic anomalies (or strongly magnetized oceanic crust [*Sibuet et al.*, 1995]), and in the Galicia Bank region it is overlain on its east flank by sediments interpreted as synrift in origin [*Beslier et al.*, 1993]. Its formation has been associated with the final stages of rifting and the initiation of seafloor spreading [*Boillot et al.*, 1995b; *Sibuet*, 1992]. Adjacent to the continental rise and the southern flank of Galicia Bank, fault-bounded basement blocks are observed which were sampled at ODP Sites 901 and 1065 [*ODP Leg 173 Shipboard Scientific Party*, 1998]. On multichannel seismic (MCS) profile LG-12 [*Krawczyk et al.*, 1996] the bounding faults verge downward onto a low-angle reflection event, which has been called the H reflector. H is very similar in appearance to the S reflector on the Galicia Bank, which has been used as evidence for detachment or décollement tectonics in the evolution of that region of the West Iberia margin [e.g., *Hoffmann and Reston*, 1992; *Krawczyk and Reston*, 1995]. Preliminary studies of the H reflector [*Krawczyk et al.*, 1996] have suggested a similar form of deformation for the southern IAP part of the margin.

A suite of holes drilled into acoustic basement by the Ocean Drilling Program Legs 149 and 173 along a profile located south of Galicia Bank, at the northern side of the southern IAP, is thought to cross the entire ocean-continent transition [*ODP Leg 173 Shipboard Scientific Party*, 1998] (Figure 2). Starting from the continental end and traversing oceanward, Sites 901, 1065, and 1069 recovered sedimentary rocks and fossil evidence indicative of a shallow water, continental shelf environment. Sites 1067, 900, and 1068, all within 2 km of each other, sampled possible lower continental crust, possible synrift melt products, and serpentinized peridotite,

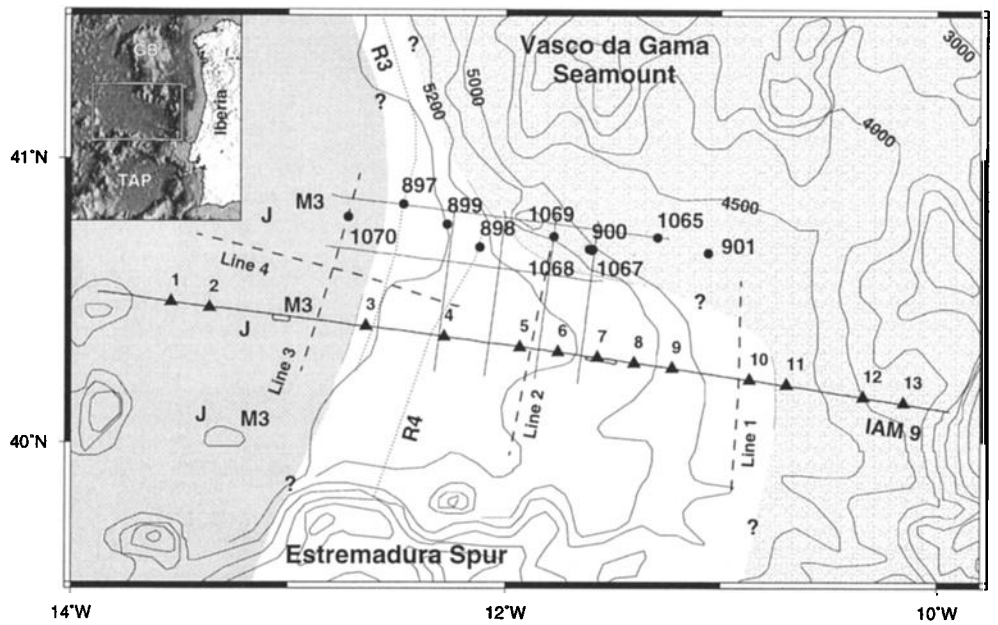

Figure 2. Bathymetry in the Iberia Abyssal Plain, contoured in 100-m intervals [*British Oceanographic Data Centre*, 1997]. The inset shows illuminated bathymetry [*National Geophysical Data Center*, 1988] for the West Iberia Atlantic margin and locates the study area in the southern Iberia Abyssal Plain; GB, Galicia Bank; TAP, Tagus Abyssal Plain. Numbered triangles locate ocean bottom seismographs that recorded useful data along the coincident IAM-9/CAM 127 seismic reflection profiles. Thin lines mark shooting tracks for this study and that of *Chian et al.* [1999]. Dashed lines mark refraction lines 1–4 of *Whitmarsh et al.* [1990]. R is Peridotite Ridge segments 3 and 4 interpreted from seismic reflection profiles [*Pickup et al.*, 1996] and direct sampling. J marks the J magnetic anomaly, and M3 marks the M3 seafloor spreading magnetic anomaly [*Whitmarsh and Miles*, 1995]. Circles denote Ocean Drilling Program sites from Legs 149 and 173. The stippled area marks the oceanward extent of thinned continental crust, and the shaded area marks the landward extent of oceanic crust, based on this paper, *Chian et al.* [1999], *Whitmarsh et al.* [1990], and *Whitmarsh and Miles* [1995].

respectively. From wide-angle seismic modeling [*Chian et al.*, 1999], Site 900 lies close to a north to south transition from thinned continental crust to what is interpreted as basement of mainly serpentinized peridotite. This interpretation is consistent with the drilling results which suggest this site could represent a tectonic window into lower continental crust but is inconsistent with the tentative interpretation of anomalously raised heat flow measurements [*Louden et al.*, 1997] that this site lies over at least 2 km of continental crust. Site 899 did not sample basement but recovered a breccia of serpentinite and serpentinized peridotite, while Site 897 sampled segment R3 of the peridotite ridge. Finally, Site 1070, 20 km oceanward of the peridotite ridge but 30 km landward of the J magnetic anomaly, sampled further serpentinized peridotite intruded by veins of gabbro. This site is interpreted on geophysical evidence to be close to, or to overlie, crust created at a spreading rate of ~10 mm yr^{-1} half rate shortly after the onset of seafloor spreading.

In 1995 we carried out a detailed geophysical investigation of the transition zone in the southern IAP between 40°N and 41°N during *Discovery* Cruise 215. This region was chosen because four exploratory seismic refraction lines that had already been acquired, as well as the identification of probable seafloor spreading anomalies, gave tentative indications of the extent of the transition zone and of the oceanic and thinned continental crusts. Further, five ODP sites, together with site survey reflection profiles, had already been occupied there [*Sawyer et al.*, 1994]. The particular profile reported here is coincident with a preexisting deep multichannel seismic reflection profile, IAM-9 [*Banda et al.*, 1995] (Figures 3 and 4) and ~40 km south of the ODP Legs 149 and 173 drilling transect. On IAM-9, no prominent low-angle reflection events similar to H and S are identified within crystalline basement, and a 130-km-wide transition zone separates fault-bounded blocks of continental crust from segment R4 of the peridotite ridge [*Pickup et al.*, 1996]. Seismic reflection profiles, including IAM-9 located in the transition zone, are characterized by two distinct laterally continuous layers defined by their reflectivity. A weakly reflective basement and 1–2 km thick upper layer and a highly reflective subbasement layer are identified [*Pickup et al.*, 1996]. Basement topography is generally more sub-

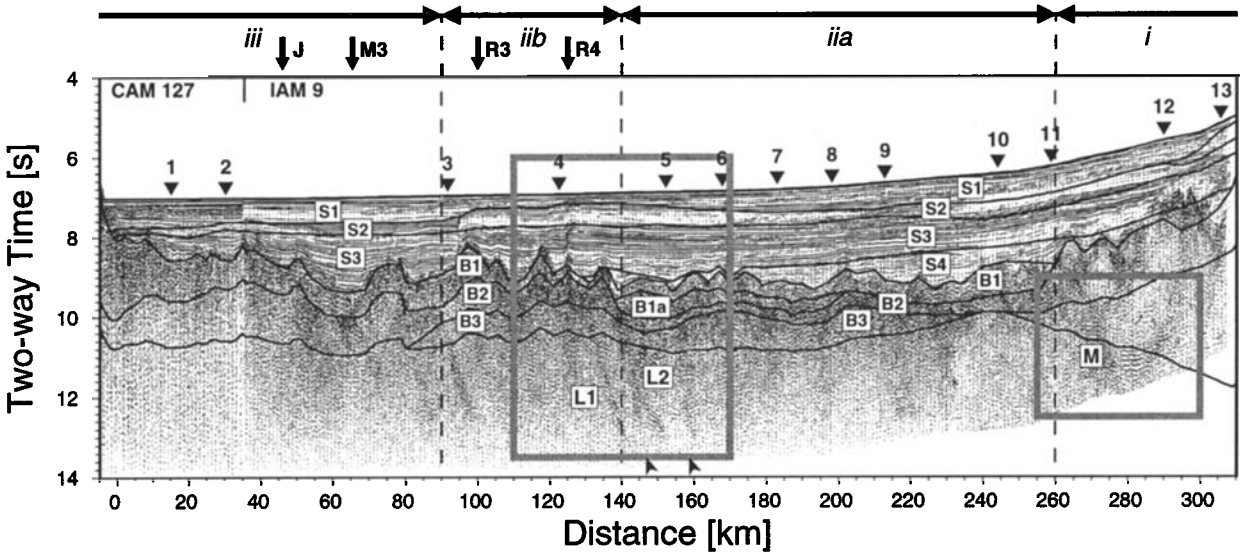

Figure 3. Time-migrated multichannel seismic reflection profiles IAM-9 and CAM 127 coincident with the seismic refraction profile in Figure 2 with refraction velocity model layer boundaries overlain (Figure 7a). Dashed lines bound regions i, iia, iib, and iii used to describe the velocity model. Velocity model sediment layers labeled S1–S4 and basement layers labeled B1–B3 in region ii are described in the text; layers B1 and B1a appear to coincide with an "unreflective" upper basement layer [*Pickup et al.*, 1996]. OBS and OBH instrument locations are indicated by triangles along the top of the section. J marks the J magnetic anomaly, and M3 marks the M3 seafloor spreading magnetic anomaly [*Whitmarsh and Miles*, 1995]. Boxes identify regions enlarged in 4A and 4B. Vertical exaggeration is 3.5:1 at 6 km s^{-1}.

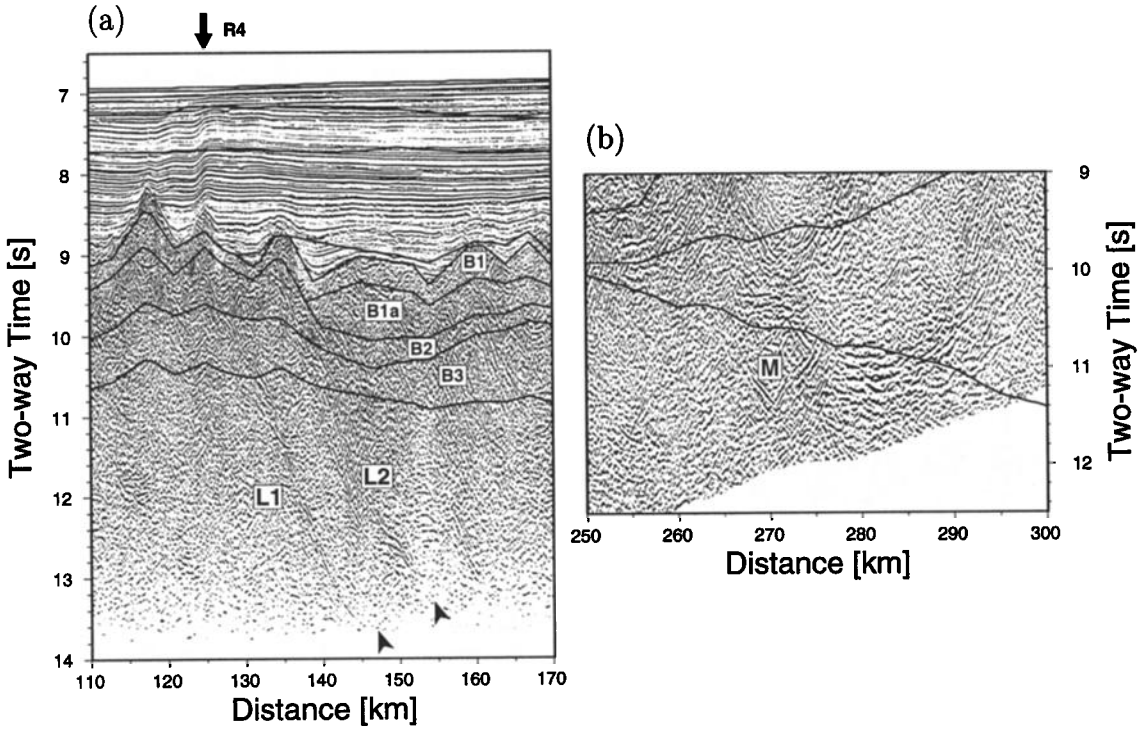

Figure 4. Enlarged sections from Figure 3. (a) Steep dipping crustal reflectors L1 and L2 are visible down to 13.5 s two-way time (twt) where the sea bottom multiple has been muted [*Pickup et al.*, 1996]. (b) The strong reflector M [*Pickup et al.*, 1996] beneath fault-rotated blocks of continental crust (265–285 model km) coincides with the Moho determined from the wide-angle model where the crust begins to thicken below the lower continental slope. Vertical exaggeration is 3.5:1 at 6 km s^{-1} for both sections.

dued in the transition zone than over the oceanic crust [*Discovery 215 Working Group*, 1998]. Unlike the offsets between segments R1, R2, and R3, in the IAM-9 profile, segments R3 and R4 appear to overlap. To the north, the transition zone reduces in width [*Pickup et al.*, 1996; *Chian et al.*, 1999] until west of the Galicia Bank, faulted blocks of continental crust appear to almost directly abut the peridotite ridge [*Boillot et al.*, 1980].

The four wide-angle seismic profiles of *Whitmarsh et al.* [1990] provided prior indications on the deep velocity structure in the southern IAP. Three of the lines (1, 2, and 3) are aligned north-south and intersect our profile (Figure 2). Lines 1 and 2 are both located within the transition zone and were interpreted in terms of a thin continental crust, <4 km thick [*Whitmarsh et al.*, 1990]. In Line 1, only 80 km west of the continental shelf, the thin crust directly overlies normal mantle velocities of ~8 km s^{-1}. Line 2, 80 km farther west and 30 km from the R4 peridotite ridge, was interpreted in terms of a 5-km-thick high-velocity lower crustal layer with velocity >7 km s^{-1}. Line 3 lies ~30 km oceanward of the R3 peridotite ridge. Here, and along line 4 west of R3, normal oceanic layer 2 velocities are measured between 4.0 and 5.4 km s^{-1}, but the velocities measured for the lower crust of 7.55–7.7 km s^{-1} are somewhat higher than normal for oceanic layer 3 [*Mutter and Mutter*, 1993].

Our new data essentially confirm the above velocity structures but, more importantly, provide a detailed and well-constrained velocity structure along the IAM-9 profile. This structure allows the essential characteristics of four distinct zones along the profile to be described. These are, from west to east, oceanic crust, peridotite ridge overlap, transition zone, and thinned continental crust. Our interpretation differs from that of *Whitmarsh et al.* [1990] in the vicinity of lines 1 and 2. We draw significant new conclusions about the development of the West Iberia margin from these, and other, data.

2. Experimental Procedure and Data Processing

Wide-angle seismic data were acquired together with normal incidence multichannel seismic (MCS), surface gravity and surface and deep-towed magnetic data during RRS *Discovery* Cruise 215 [*Discovery 215 Working Group*, 1998]. A total of 39 ocean bottom instrument deployments were made during two experiments. Results presented here are from the first full deployment of instruments along a 350-km line between 9°55'W and 13°55'W at ~40°20'N, following the same ship-track as the deep seismic reflection profile IAM-9 (Figure 2). The second experiment recorded both MCS and wide-angle seismic data along profiles located further north. Here, a 4×4 grid of ocean bottom instruments oriented along N–S and E–W lines and spaced ~20 km apart extended south to intersect the 40°20'N profile. The seismic structures along two northern E–W lines and four N–S lines in Figure 2 that lie just south of Vasco da Gama seamount and on either side of the Ocean Drilling Program Legs 149 and 173 drill sites have been presented by *Chian et al.* [1999].

The profile at 40°20'N extends from the base of the continental slope to unambiguous oceanic crust and traverses the entire ocean-continent transition (OCT) zone in the Iberia Abyssal Plain. It is bounded at the west end by a small seamount at 14°W and to the east by the Portuguese continental slope at 10°W. It crosses seafloor spreading magnetic anomalies and the J magnetic anomaly [e.g., *Whitmarsh and Miles*, 1995], the overlap of segments R3 and R4 of the peridotite ridge, and faulted blocks of thinned continental crust [*Pickup et al.*, 1996]. A total of 13 ocean bottom instruments recorded useful data (Figure 2). These consisted of Dalhousie three-component geophone/hydrophone (ocean bottom seismometers (OBS)) and Cambridge hydrophone (ocean bottom hydrophone (OBH)) packages (Table 2). An air gun seismic source was used, comprising a 6346 cubic inch (~104 L), 12-gun tuned array, fired approximately every 100 m at a depth of 20 m. This gave a seismic source rich in low frequencies which was successfully recorded at offsets up to 180 km. The spacing between recording instruments varied along the line, but in the OCT an average of 15 km was achieved. All positional information came from the shipboard Global Positioning System (GPS) equipment.

Preprocessing of wide-angle seismic data for travel-time picking involved making clock drift corrections (of the order of 10 ms) to adjust the clock in each instrument to a GPS time base. Instrument locations were corrected for any shift from the lay position during the ~5 km descent through the water column by minimizing the least squares misfit between the observed water wave arrivals and those calculated for the bathymetry and sound speed model. After correction the instruments lie a maximum distance of 420 m out of the plane of the profile, with a mean distance of 110 m. The out of plane distance does not significantly affect the interpretation. Source-instrument offsets were smoothed to reduce scatter in the (nondifferential) GPS positions using an equally weighted 15-point average filter. After preprocessing, the instrument locations and source-instrument offsets have an estimated accuracy of 50 m.

Picking the onset of first and later arrivals up to 30–40 km offset (Figure 5) was accomplished without any filtering or data enhancement. The later arrivals are important to constrain the sediment and OCT velocity structure since most phases are only observed as first arrivals over a small offset range (~5 km). Sediment layers are identified in the data sections as linear phases with velocities up to 4.5 km s^{-1} which can often be traced back to normal-incidence reflections. Crustal phases have velocity >4.5 km s^{-1} and often have very

Table 2. Deployment Location and Specification of Ocean Bottom Seismic Instruments Used for Wide-Angle Modeling

Instrument	Latitude, °N	Longitude, °W	Instrument Depth, km	Hydrophone Sensor	Geophone Sensor	Sample Rate, Hz
1	40°29.83'	13° 32.36'	5.30	√		256
2	40°28.56'	13°21.77'	5.30	√	√	173
3	40°24.69'	12°38.66'	5.24	√	√	173
4	40°22.39'	12°17.07'	5.22	√	√	173
5	40°20.17'	11°56.15'	5.18	√		256
6	40°19.12'	11°45.46'	5.16	√	√	173
7	40°18.00'	11°34.46'	5.12	√		128
8	40°16.82'	11°24.26'	5.09	√	√	173
9	40°15.70'	11°13.70'	5.01	√		128
10	40°13.20'	10°52.16'	4.81	√		128
11	40°12.16'	10°41.90'	4.70	√		256
12	40° 9.54'	10°20.58'	4.19	√		128
13	40° 8.30'	10° 9.32'	3.89	√		256

variable travel times due to the basement topography. At offsets >40 km a band-pass filter of 3–25 Hz was used to increase the signal-to-noise ratio (SNR) and the application of an 8 km s^{-1} reduction velocity enhances the correlation of the lower crustal/upper mantle phases (Figure 6). Upper mantle arrivals are horizontal in the reduced sections, with deep basement phases at a slightly lower velocity but with a higher amplitude. Where available, the vertical geophone channel was used, since this exhibits a better SNR at large offsets

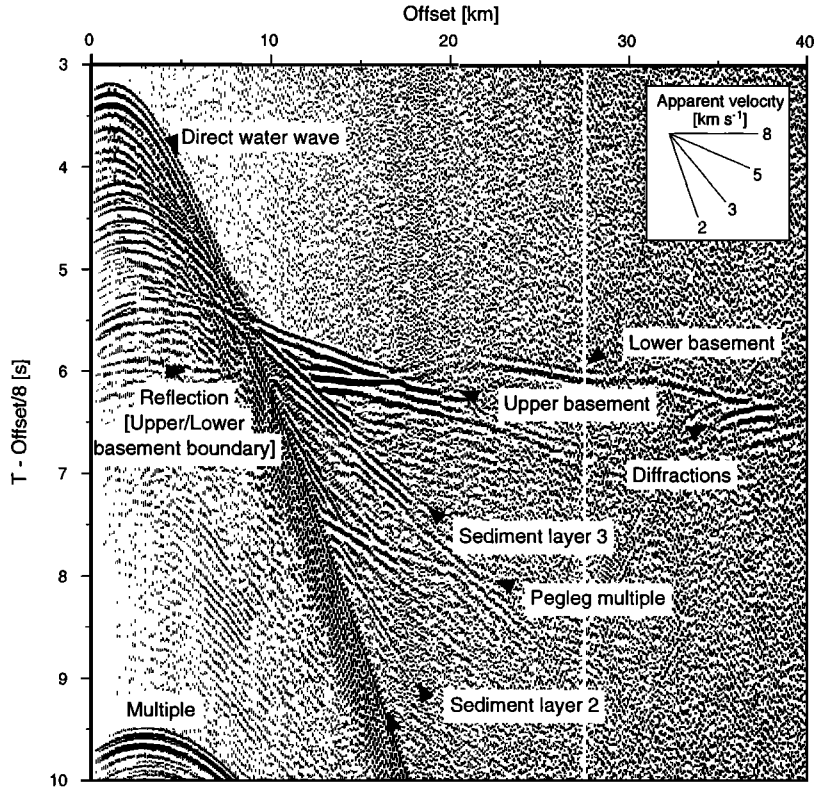

Figure 5. Hydrophone record section of instrument 10 located over transitional basement with continental crust 15 km to the east (right), band-pass-filtered 3–25 Hz with time reduced at 8 km s^{-1} and gain proportional to offset. Lower basement refracted arrivals are observed up to 40 km offset, but no upper mantle arrivals are observed in this section where the crust thickens toward the continental slope. Severe basement topography causes travel time and amplitude variations in the lower basement arrivals where basement highs cause early, but low-amplitude (defocused) refracted arrivals.

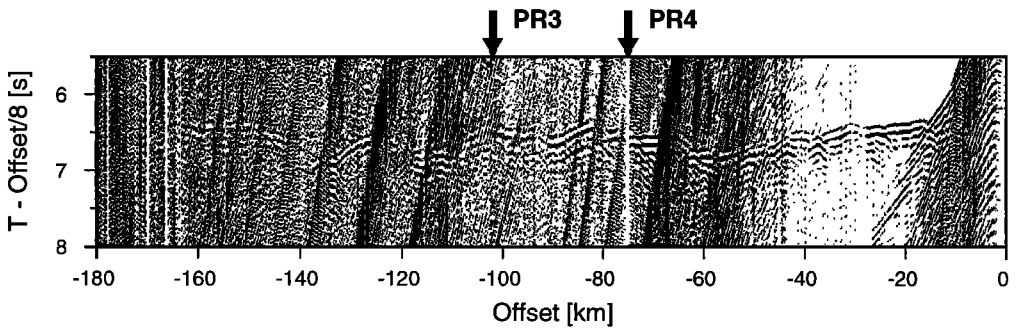

Figure 6. Vertical geophone record section of instrument 8 located 198 km along the profile, band-pass-filtered 3–25 Hz, with time reduced at 8 km s^{-1} and with gain proportional to offset. The tuned air gun array produced a high-energy, low-frequency source which allowed travel time picks to offsets of 180 km. The near-vertical stripes are water wave multiples from earlier shots.

(>50 km) when compared to the hydrophone channel. An exception is at near-normal incidence when identifying reflections. Here, the vertical geophone channel was observed to saturate with the direct water wave arrival, but the hydrophone does not. Hence any picks after the direct water wave arrival were made from the hydrophone channel.

Travel time uncertainties include the uncertainty in picking arrivals, in the instrument clock, and in the instrument and source location. Picking uncertainty, the largest single source of uncertainty, generally increases with offset as the SNR reduces. The picking uncertainty for all refracted arrivals is estimated by a function which increases linearly with offset from 10 ms at 0 km offset to a maximum of 125 ms, equal to one period of the source wavelet, at 115 km offset. Since reflected phases are all second arrivals, they are assigned a larger uncertainty of 62.5 ms, equal to half the period of the source wavelet. A complete set of OBS record sections, in digital SEGY format, is available in the electronic supplement[1].

3. Two-Dimensional Velocity Structure From Travel Time Modeling and Synthetics

We employed the two-dimensional ray tracing of *Zelt and Smith* [1992] for inversion/forward modeling from the top of the model down. The velocity model is defined in layers using depth and velocity nodes. Depth nodes set the topography of each layer; velocity nodes control the velocity at the top and bottom of each layer and hence the velocity gradient within each layer and whether there is a step in velocity between layers. In general, more depth nodes are defined than velocity nodes since in modeling we try to keep lateral velocity variations to a minimum. First, the water layer and the sediment layer thickness and velocities were modeled using refracted and wide-angle reflected phases observed by the ocean bottom instruments, then the rugged basement topography was adjusted to fit the normal-incidence travel times before finally wide-angle reflected and refracted phases from the basement and upper mantle were modeled. The sediment layers are relatively flat with small lateral velocity variations. Velocity and depth nodes every 10–20 km were successfully included in the travel-time inversion. The basement layers are described in four regions (i, iia, iib, and iii), defined by lateral changes in the seismic velocity, reflective character, and magnetic features (Figure 7a). The complex basement topography required depth nodes every 3–5 km. Dense picking (<2 km) of the basement reflection at normal incidence gave a successful inversion of this boundary. To match travel time variations with offset for intrabasement/upper mantle wide-angle arrivals, the intrabasement layers need to follow the basement topography. This requires a large number of depth nodes for these layers and causes the inversion from wide-angle data to be generally unstable. Inversion was successful for the deep basement velocities, the Moho depth, and the upper mantle velocity, but the basement layer boundaries had to be determined by forward modeling.

Synthetic seismograms were calculated using the asymptotic ray theory code of *Zelt and Forsyth* [1994]. This allows us to make a qualitative comparison with amplitude variations in the recorded data and to confirm our phase identifications. For consistency, we choose to use the same convolutional wavelet for all our synthetic sections, a band-pass-filtered derivative of the Ricker wavelet for positive times. P wave quality factors Q, which determine anelastic attenuation, are taken from estimates based on seismic reflection data recorded across Galicia Bank [*Boillot et al.*, 1995b]. Q values vary between 100 and 200 for the sediment layers, 650 for shallow basement phases, 900 for the deepest

[1]Supporting OBS record sections are available on diskette or via Anonymous FTP from kosmos.agu.org, directory APEND (Username = anonymous, Password = guest). Diskette may be ordered from American Geophysical Union, 2000 Florida Avenue, N.W., Washington, DC 20009 or by phone at 800-966-2481; $15.00. Payment must accompany order.

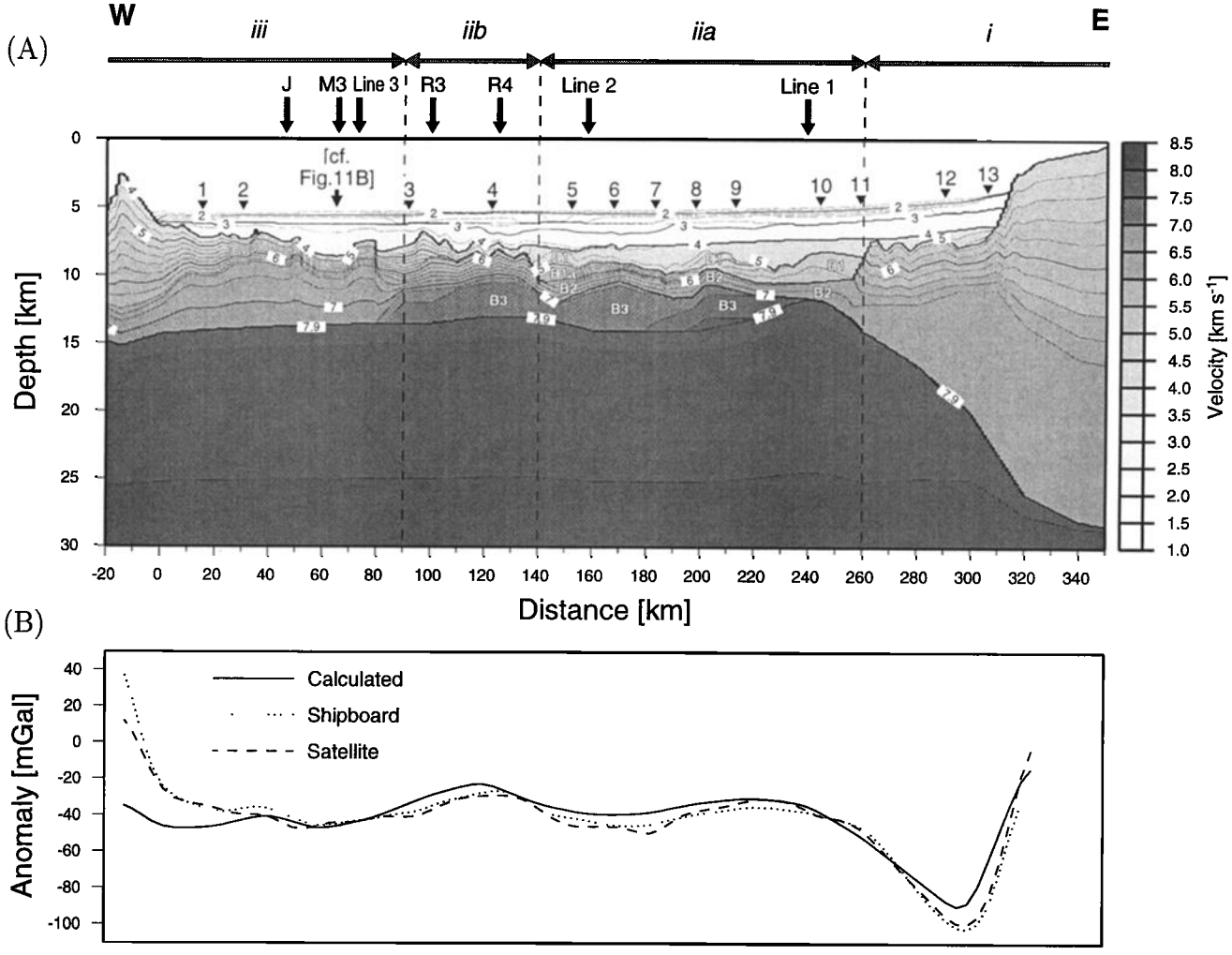

Figure 7. (a) Two-dimensional P wave velocity model (5× vertical exaggeration) for the Iberia Atlantic margin at 40°20'N contoured every 0.2 km s^{-1} from 13 wide-angle seismic instruments, located with triangles. The velocity model is described and interpreted in the text in four sections, i, iia, iib, and iii, bounded with dashed lines. Basement layers labeled B1–B3 in region ii are described in the text. (b) Gravity anomaly observed at the sea surface, derived from satellite altimetry [*Sandwell and Smith*, 1997] and from converting the velocity model to density using the relationship of *Ludwig et al.* [1970]. Significant differences occur between calculated and observed anomalies in the vicinity of the subcircular seamount bounding the western end of the profile due to the assumed infinite extent of the density model out of the plane of the profile (see text).

basement phases, and 1000 for unaltered upper mantle peridotite. A Poisson's ratio of 0.25 was used for all layers. Velocity was related to density using the same relationship as for our gravity modeling (see section 5).

3.1. Sediment Velocities

Four layers corresponding to sediments were used to fit the wide-angle data. Three main sediment refracted phases (layers S2, S3, and S4) were identified with velocities of 2.3, 3.0, and 4.5 km s^{-1}, with a small velocity gradient in each corresponding layer. A fourth layer (layer S1) was introduced between the seafloor and layer S2, with a linear velocity gradient from water velocity (1.52 km s^{-1}) to that of the velocity of the first refracting layer (~2.3 km s^{-1}). This shallow sediment velocity structure is in agreement with shipboard velocity measurements on the ODP Leg 149 drill cores [*Harry and Batzle*, 1996]. While layers S1, S2, and S3 extend across the whole profile, layer S4 is not observed overlying oceanic crust. At its maximum thickness the top of layer S4 is 2 km above the basement topography, but as the basement shallows at the continental slope and oceanward toward the peridotite ridge, layer S4 thins and cannot be resolved from the wide-angle seismic data. Reflections from the top of the 3.0 km s^{-1} (layer S3) and 4.5 km s^{-1} (layer S4) layers are identified at near normal incidence in the hydrophone channel of some instruments, but arrival times are difficult to pick since they are not first arrivals. The reflections provide a strong constraint on layer thickness, with a

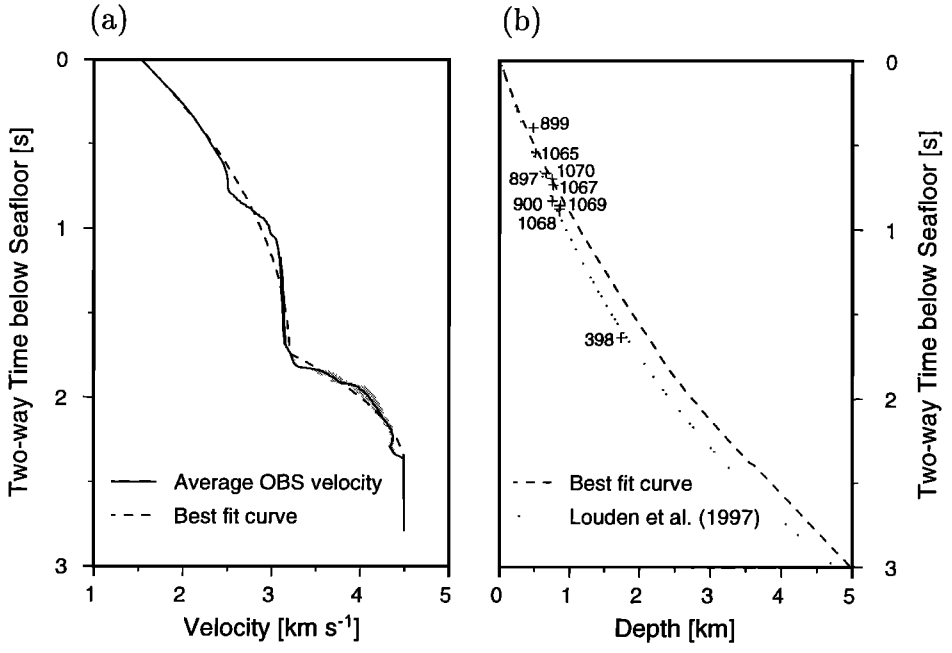

Figure 8. (a) Sediment velocity structure from the wide-angle velocity model, compiled by averaging 1-D velocity profiles spaced every 1 km along the profile. Two second-order polynomials form a best fit velocity-time function: $-0.5279T^2 + 1.8884T + 1.52$ for travel time (T) less than 1.739 s; $-2.7871T^2 + 13.495T - 11.831$ for travel time (T) between 1.739 s and 2.381 s; travel times (T) >2.381 s have a constant velocity of 4.5 km s^{-1}. (b) Two-way time to depth relationship for the best fit wide-angle velocity structure (dashed line) and *Louden et al.* [1997] (dotted line) based on basement penetrating boreholes (crosses) and sonobuoy velocity analysis [*Whitmarsh et al.*, 1990]. The best fit depth-time function converted from Figure 8a is $-0.088T^3 + 0.472T^2 + 0.760T$ for travel time (T) less than 1.739 s; $-0.465T^3 + 3.374T^2 - 5.916T + 4.814$ for travel time (T) between 1.739 s and 2.381 s; 2.250T-1.772 for travel time (T) greater than 2.381 s.

maximum of 0.5 km for layer S2, thinner than layer S3 which is up to 2.3 km. When our final velocity model boundaries are overlaid on the coincident reflection profile (Figures 3 and 4), the top boundaries of the 3.0 and 4.5 km s^{-1} layers (layers S3 and S4, respectively) closely follow reflections, while the upper boundary of the 2.3 km s^{-1} layer (layer S2) crosses reflectors where the layer thickens over the region of the overlapping peridotite ridges.

Figure 8a shows the mean wide-angle seismic velocity structure for the sediment layers. This is calculated by converting one-dimensional (1-D) velocity profiles every 1 km along the full length of the velocity model to two-way time, shifting the origin to the seabed and then taking a mean. Two second-order polynomial functions are used to fit this profile and calculate a two-way time to depth relationship (Figure 8b). The relationship gives a close approximation to the directly observed depth of acoustic basement from Leg 149 and Leg 173 of the Ocean Drilling Program but overestimates the depth to basement for Deep Sea Drilling Project (DSDP) Site 398 [*Sibuet et al.*, 1979]. Site 398 is adjacent to Vigo Seamount, where basement is nearly 1 s (two-way time) deeper than Site 900, the deepest basement sampled by the Ocean Drilling Program in Leg 149. We suggest that the discrepancy in basement depth may be attributed to a thicker accumulation of low-velocity sediments at the edge of the abyssal plain, in a more proximal location to the source.

3.2. Region i

East of 10°45'W (a model distance of ~260 km; Figure 7a), we observe a sharp increase in basement relief and a lateral increase in upper crustal velocity in the wide-angle seismic data. Instrument 11 straddles this lateral change, and first arrivals from crustal turning rays are up to 500 ms earlier to the east of the instrument than to the west, for the same offset (Figure 9e). This coincides with the interpretation of rotated blocks of faulted continental crust and the occurrence of a Moho reflection in the coincident deep seismic reflection section IAM-9 [*Pickup et al.*, 1996]. We model the upper crust between 10°45'W and the base of the continental slope from the wide-angle seismic data (Figure 9) with a single layer ~4 km thick and a vertical velocity gradient (~0.33 s^{-1}) from 5.5 to 6.8 km s^{-1}. This layer is constrained by reversed turning rays to three instruments. The velocity structure of the lower

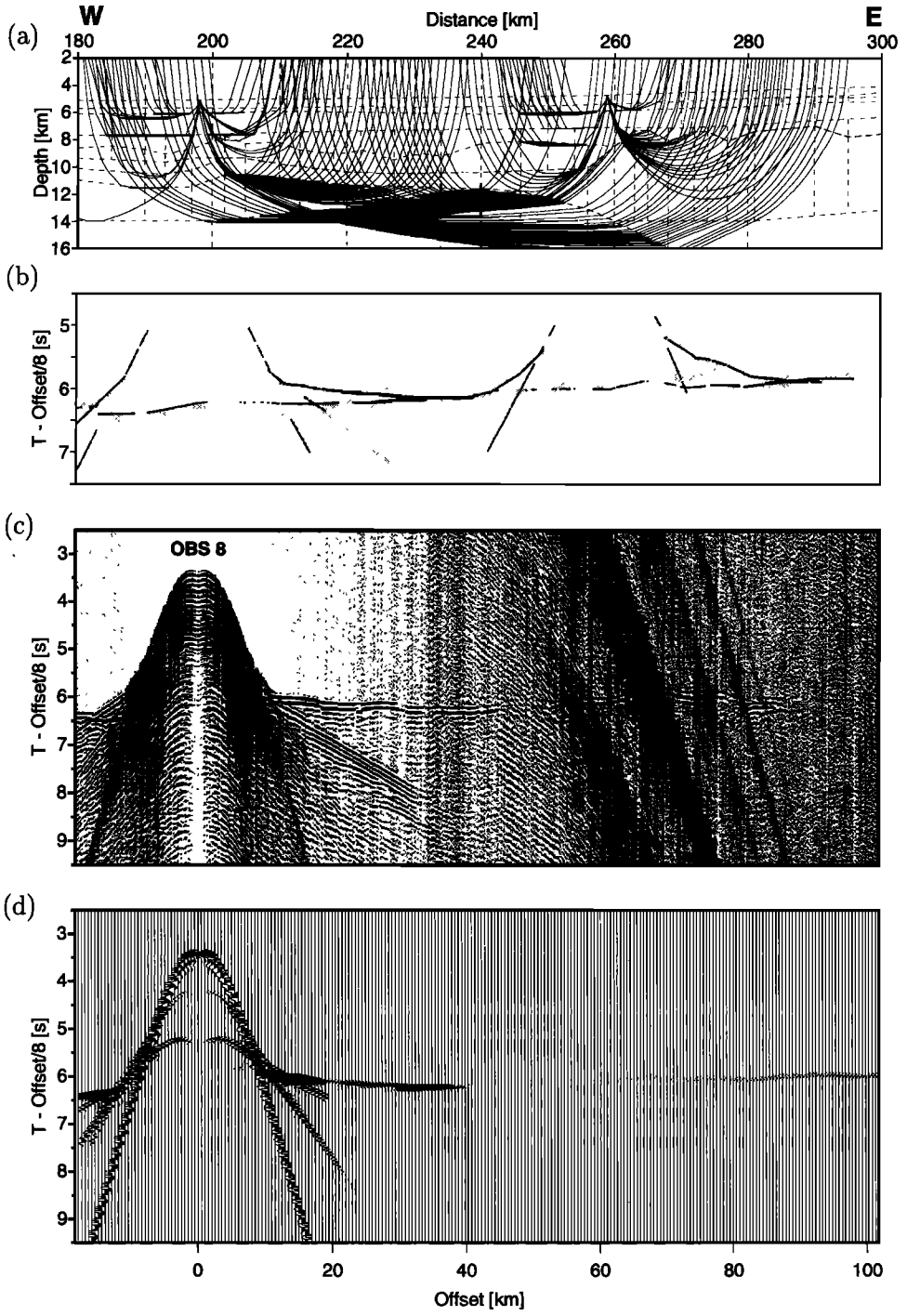

Figure 9. (a) Ray geometry (see text for method) through the transition zone and thinned continental crust for picked phases only (1 in 10 rays plotted) for instruments 8 and 11. (b) Travel time picks (shaded bars) and calculated arrival times (solid) reduced at 8 km s^{-1}. The height of the bars shows the estimated error, which ranges from 30 to 100 ms. (c) Vertical geophone record section for instrument 8, band-pass-filtered 3–25 Hz with time reduced at 8 km s^{-1} and gain proportional to offset. (d) Synthetic seismograms for instrument 8 calculated by ray tracing the velocity model in Figure 7a with gain proportional to offset. (e) Hydrophone record section for instrument 11, band-pass-filtered 3–25 Hz with time reduced at 8 km s^{-1} and gain proportional to offset. (f) Synthetic seismograms for instrument 11 calculated by ray tracing the velocity model in Figure 7a with gain proportional to offset.

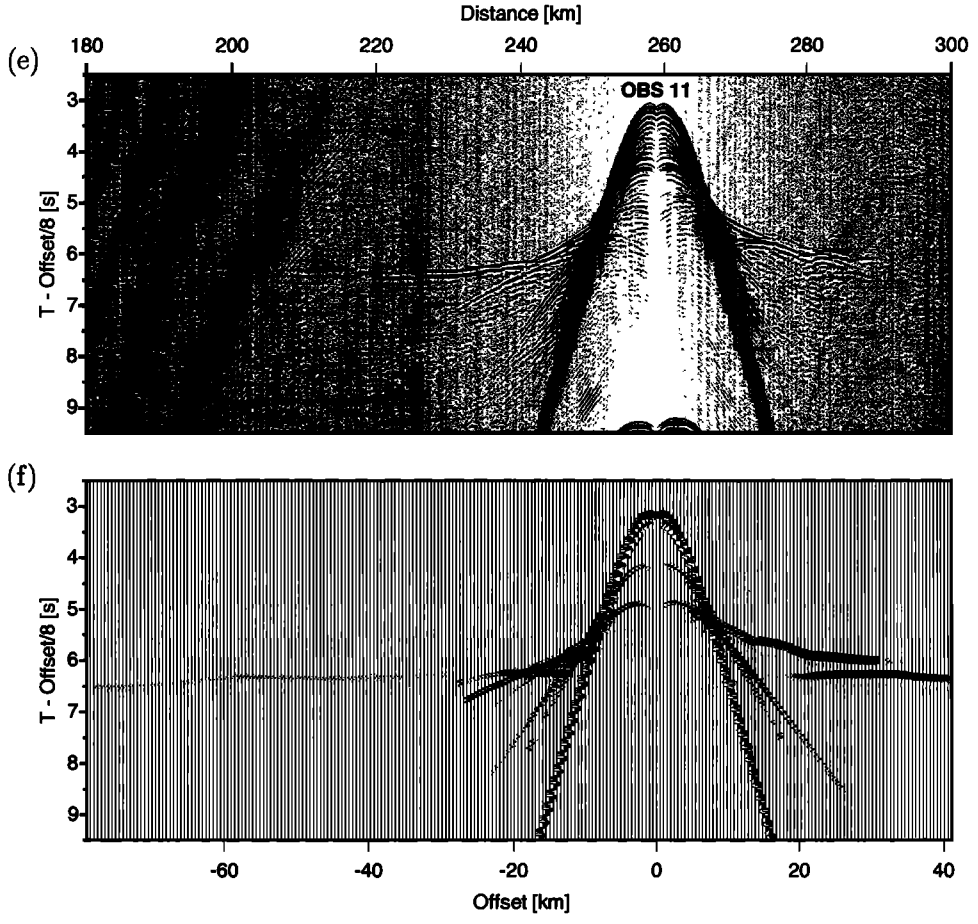

Figure 9. (continued)

crust adjacent to the continental slope and shelf is not constrained from the seismic data because no seismic receivers were deployed on the continental shelf. The crustal thickness in this region is modeled using gravity data (see section 3.3).

3.3. Region ii

Wide-angle seismic data from instruments located between 12°40' and 10°45'W (90 and 260 model km) show strong lateral travel time variations in refracted arrivals mainly from layers with velocity >7.0 km s^{-1} (Figures 2, 6, 9, and 10). Layers with velocity <7.0 km s^{-1} are relatively thin since refracted arrivals are only identified as first arrivals over limited offsets (typically between 10 and 15 km). This region is subdivided into region iia, referred to as the transition zone [e.g., *Pickup et al.*, 1996; *Discovery 215 Working Group*, 1998; *Chian et al.*, 1999], and region iib, the overlapping peridotite ridges. The basement and upper mantle velocity structure is modeled using three gradient layers which are continuous across the region (layers B1, B2 and B3; Figure 3) and a single, high gradient layer (layer B1a), which is not observed beneath the peridotite ridges and thins laterally toward the continent, under the eastern third of this region. Broadly, the velocity structure in region ii (Figure 11a) is a high gradient (~1 s^{-1}) layer ~3 km thick (layers B1, B1a, and B2), overlying a low gradient (~0.2 s^{-1}) layer up to 4 km thick (layer B3).

The top basement layer B1 increases in thickness and velocity from 1 km thick and 4.3 km s^{-1} in region iib to 2 km thick and 5.2 km s^{-1} in region iia, adjacent to the faulted blocks of continental crust. The velocity gradient is <0.5 s^{-1}, and in general, refracted arrivals from this layer are indistinguishable in velocity from the deepest sediment layer. The vertical transition in velocity between layer B1 and layer B2 varies considerably across the transition zone. In region iib it is modeled as a velocity step of 1 km s^{-1}. In region iia, directly adjacent to the peridotite ridges, there is an ~2-km-thick high-velocity-gradient (layer B1a) between layer B1 and layer B2 with no steps in velocity. Layer B1a reduces in thickness toward the continent over 60 km, with increasing velocity gradient until it becomes a step of 1 km s^{-1} off which we observe reflections (Figure 5), adjacent to the thinned continental crust. In region iib, layer B2 is 2 km thick and has a velocity of 5.7–7.3 km s^{-1} (gradient of ~0.8 s^{-1}). In region iia, layer B2 has a laterally invariant velocity structure (6.4–7.0 km s^{-1}) and thickness (1 km).

The peridotite ridges, region iib, have a very similar velocity structure to region iia (Figure 11a). However, since layer B1 is ~1 km thinner and the basement is

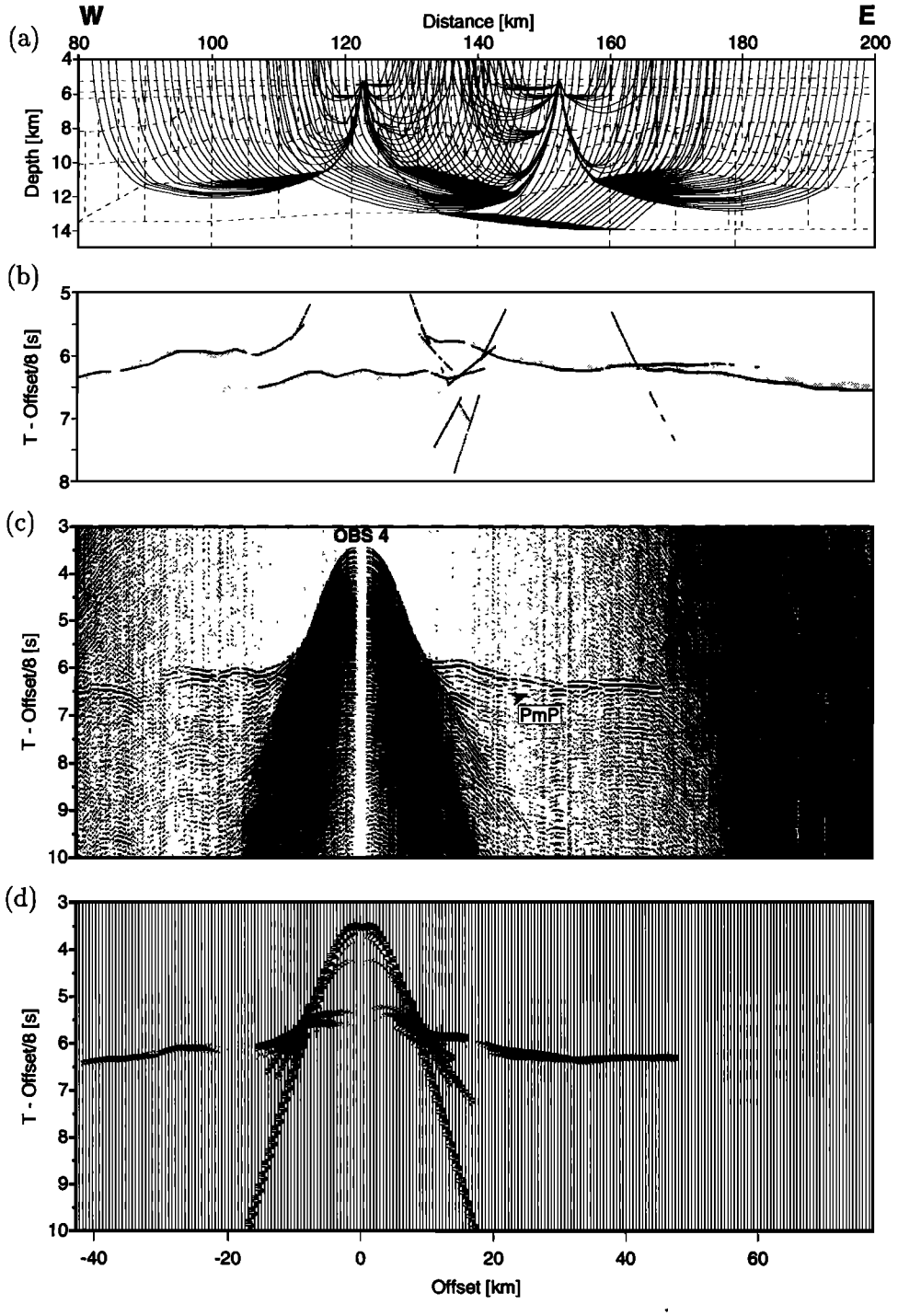

Figure 10. (a) Ray geometry (see text for method) through the peridotite ridge for picked phases only (1 in 10 rays plotted) for instruments 4 and 5. (b) Travel time picks (shaded bars) and calculated arrival times (solid) reduced at 8 km s^{-1}. The height of the bars shows the estimated error, which ranges from 30 to 100 ms. (c) Vertical geophone record section for instrument 4, band-pass-filtered 3–25 Hz with time reduced at 8 km s^{-1} and gain proportional to offset. (d) Synthetic seismograms for instrument 4 calculated by ray tracing the velocity model in Figure 7a with gain proportional to offset. (e) Hydrophone record section for instrument 5, band-pass-filtered 3–25 Hz with time reduced at 8 km s^{-1} and gain proportional to offset. (f) Synthetic seismograms for instrument 5 calculated by ray tracing the velocity model in Figure 7a with gain proportional to offset.

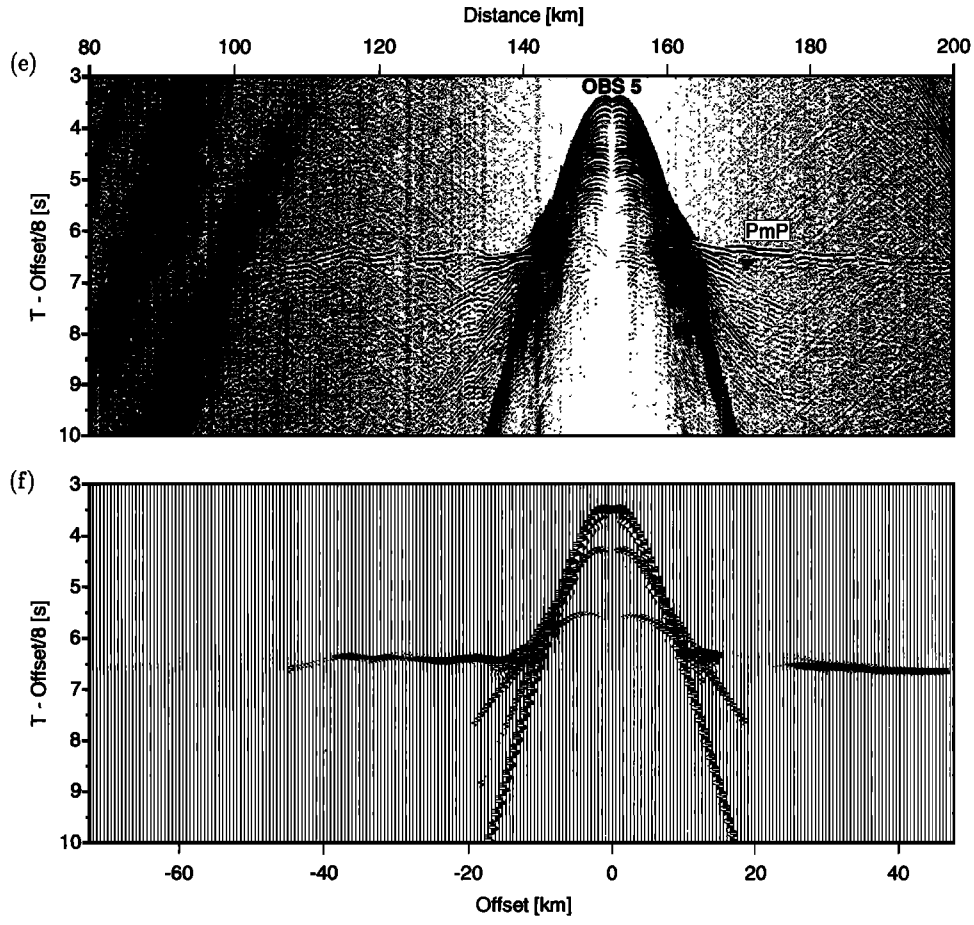

Figure 10. (continued)

significantly shallower, the velocity of the middle crust appears elevated by about 0.5 km s^{-1} (Figure 7a). Region iib extends laterally ~50 km (between 90 and 140 model km), beneath the basement highs interpreted as R3 and R4 [*Pickup et al.*, 1996] but continues ~15 km farther east than R4, with a sharp lateral velocity step into region iia. The eastern flank of segment R4 of the peridotite ridge determined from the wide-angle seismic velocity model coincides with *Pickup et al.*'s [1996] reflector L2 (Figure 4a). Synthetic seismograms for instruments lying over the peridotite ridges amplitudes show strong first-arrival amplitude variations over a distance scale of ~5 km due to the focusing effect of strong basement relief (e.g., Figures 10d and 10f). We consider that region iib, in the IAM-9 profile, may be uncharacteristically wide for the West Iberia margin due to the overlap between segments R3 and R4 of the peridotite ridge.

All instruments that recorded wide-angle seismic data to offsets >40 km show clear refracted arrivals with velocities of ~8 km s^{-1}. In most of the record sections from instruments located over region ii, we observe high-amplitude refracted arrivals at a velocity slightly lower than 8 km s^{-1} at offsets of up to 40–50 km. These arrivals are matched in the synthetic sections (Figures 9d, 10d and 10f) with a 7.3–7.9 km s^{-1} lower basement layer with a low-velocity-gradient and a thickness of up to 4 km (layer B3). There is a step of <0.5 km s^{-1} between layer B2 and layer B3 which does not cause observable reflections in the wide-angle seismic record sections. Layer B3 thins and disappears ~20 km west of where the lower continental crust starts to thicken beneath the continental slope. The Moho beneath region ii is modeled as a step of 0.15–0.4 km s^{-1} between the base of layer B3 and an upper mantle velocity of 8 km s^{-1}. The weak arrivals observed at ~30 km offset (Figures 10c and 10e) may correspond to Moho wide-angle reflections (*PmP*). Moho reflections predicted by the synthetic seismograms have travel times and amplitude very similar to the lower basement turning rays and are observed as a slight increase in amplitude at ~30 km offset (Figures 9d, 10d and 10f). The Moho has slight relief in region iib where it shallows by ~0.8 km, and beneath the continental end of region iia where the velocity at the base of layer B3 increases to 7.9 km s^{-1}.

3.4. Region iii

West of 12°40'W (at model distance ~90 km; Figures 2 and 7a) the crust is modeled with two layers

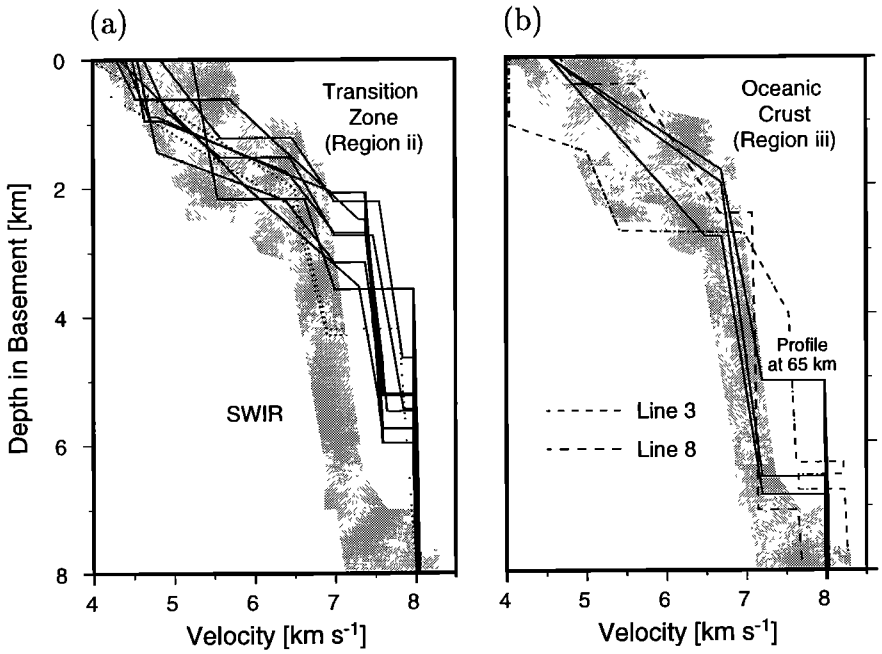

Figure 11. (a) One-dimensional velocity profiles for instruments 3 to 10, located over the transition zone (region ii), overlaid with the velocity bounds of Atlantic oceanic crust aged 59–170 Ma [*White et al.*, 1992]. Dotted lines are velocity profiles from the South-West Indian Ridge [*Muller et al.*, 1997], as an example of oceanic crust formed at slow spreading rate. (b) Same as Figure 11a, except for instruments 1 and 2, and a profile at a model distance of 65 km located over oceanic crust west of the peridotite ridges in the IAM-9 profile (region iii). Line 3 is a preexisting N–S wide-angle seismic profile which intersects the IAM-9 profile at ~73 km [*Whitmarsh et al.*, 1990] (Figure 2); line 8 is a preexisting wide-angle seismic refraction profile located west of the peridotite ridge off Galicia Bank [*Whitmarsh et al.*, 1996].

(Figures 11b and 12). Away from the seamount, a 2-km-thick upper crustal layer follows the basement topography, locally with relief >1 km. The velocity increases with depth from 4.5 to 6.5 km s^{-1}, giving a gradient of 1 s^{-1}. A lower crustal layer with velocities from 6.7 and 7.2 km s^{-1} varies between 3.5 and 4.5 km thick. At the base of the lower layer the Moho is subhorizontal at ~14 km depth and exhibits a velocity increase of ~0.8 km s^{-1}. Away from the seamount, no lateral velocity variations are observed in either layer. Synthetic seismograms (e.g., Figure 12d) show high-amplitude crustal first arrivals with a marked drop in amplitude beyond an offset of between 15 and 20 km coinciding with a change in slope of the arrivals. A clear wide-angle Moho reflection is calculated at 20 to 30 km offset which is obscured as a distinct arrival in the recorded data by an earlier refracted phase. Two subcritical reflection events are clearly observed with travel-time intercepts of 4.5 and 5.1 s from the sediment layering and the basement, respectively. The crustal velocity structure is similar to normal Atlantic oceanic crust (Figure 11b) which is consistent with the identification of seafloor spreading magnetic anomalies between 45 and 90 model km [*Whitmarsh and Miles*, 1995; *Whitmarsh et al.*, 1996].

4. Uncertainties in the Velocity Model

Statistical analysis was performed on key model parameters to provide an estimate of the uncertainty in the final velocity model. We tested the Moho depth, upper mantle velocity, and lower basement (layer B3) velocity in region i by independently perturbing each parameter (Figure 13). The Moho depth was perturbed by moving the entire boundary up and down; velocity perturbations are made so that the velocity gradient in each layer is maintained. We apply an F test on χ^2 values [*Zelt and Smith*, 1992] calculated for the final and perturbed model with the perturbed model considered different from the final model when the variation in χ^2 is significant at the 95% confidence level. The velocity uncertainty in the lower basement layer is estimated at ±0.05 km s^{-1} and in the upper mantle at -0.06/+0.2 km s^{-1}. Our preferred upper mantle velocity is slightly higher than the value with the lowest χ^2 because the higher velocity results in more travel time data points being reached by ray tracing. Error analysis on the Moho depth suggests an uncertainty of ±0.2 km, but this assumes there is no error in the overlying velocity structure. When we include the velocity uncertainty in the lower basement layer, the

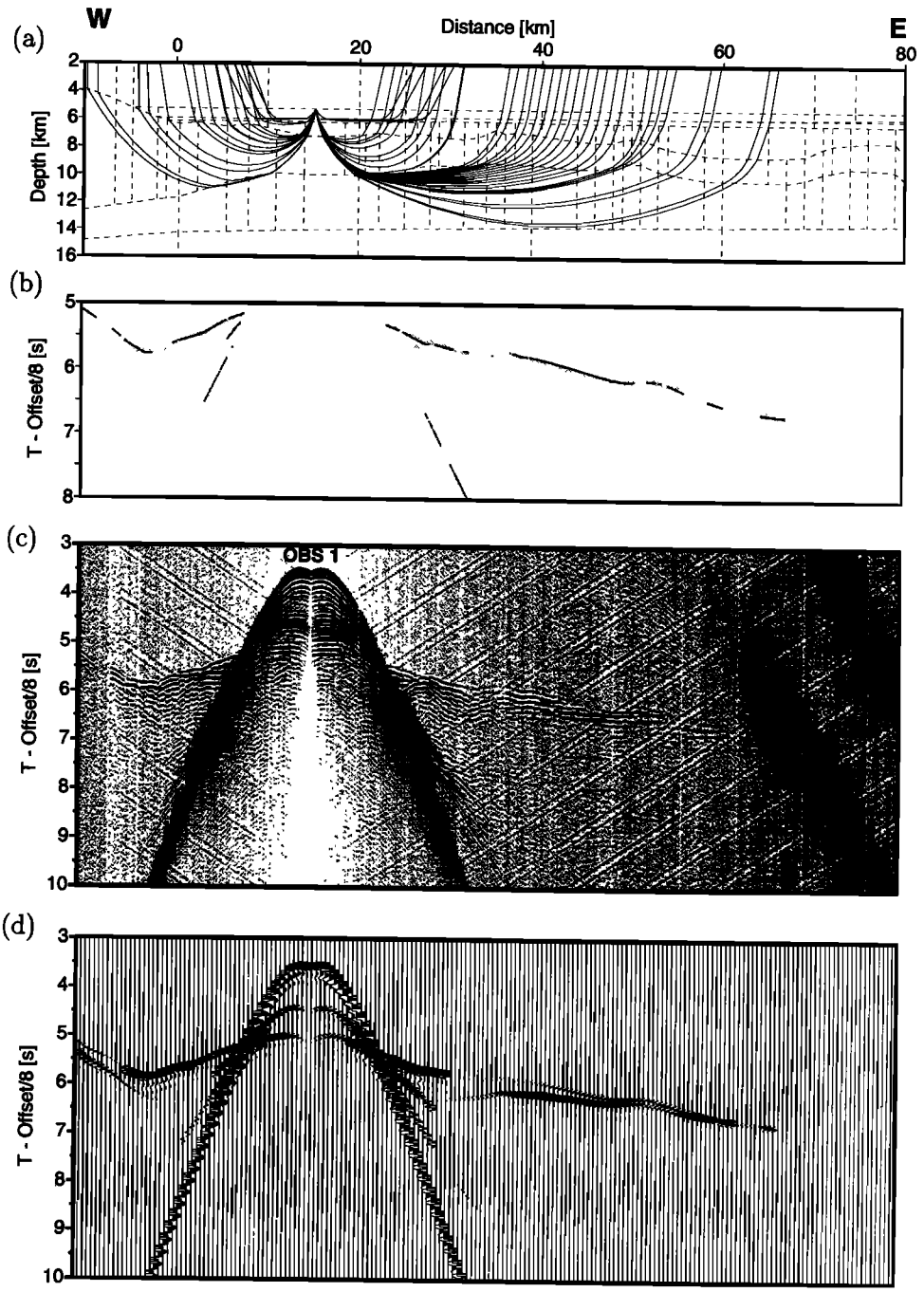

Figure 12. (a) Ray geometry (see text for method) through oceanic crust for picked phases only (1 in 10 rays plotted) for instrument 1. (b) Travel time picks (shaded bars) and calculated arrival times (solid) reduced at 8 km s^{-1}. The height of the bars shows the estimated uncertainty, which ranges from 30 to 100 ms. (c) Hydrophone record section for instrument 1, band-pass-filtered 3–25 Hz with time reduced at 8 km s^{-1} and gain proportional to offset. The linear events dipping toward 0 km offset are artifacts from the clock on this instrument. (d) Synthetic seismograms for instrument 1 calculated by ray tracing the velocity model in Figure 7a with gain proportional to offset.

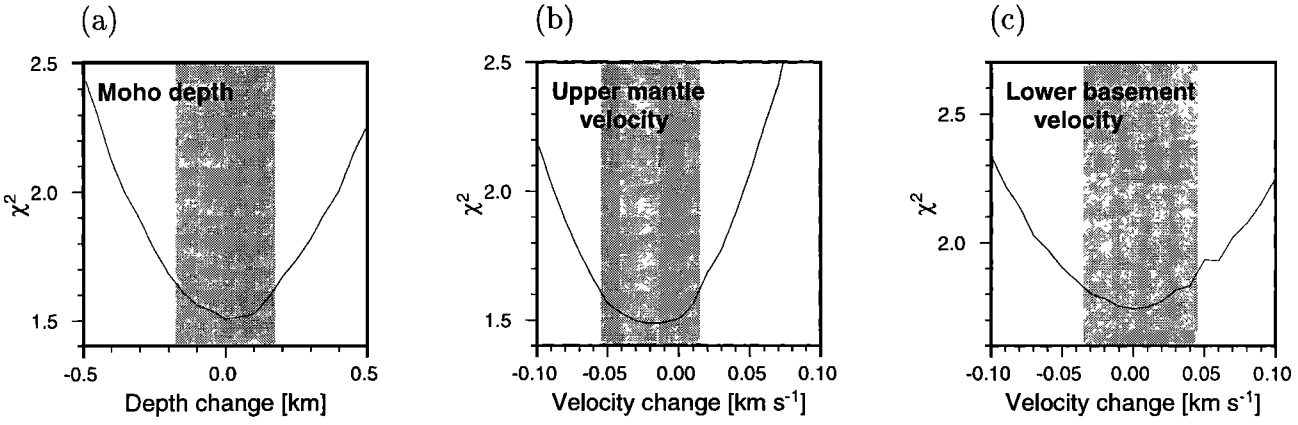

Figure 13. Uncertainty in (a) the depth of the Moho, (b) the velocity of the upper mantle, and (c) the velocity of the lower basement layer B3. Shaded areas represent the statistical 95% confidence limit of the F test (see text). We estimate the uncertainty on the Moho depth to be ±0.25 km when we include the uncertainty in the velocity of the lower basement layer.

uncertainty in the Moho depth increases to ±0.25 km. The Moho depth and upper mantle velocity uncertainties are only valid where we have ray coverage, between ~25 and 280 model km (Figure 14). The root-mean-square (RMS) residual misfit between all observed and calculated travel times for the final velocity model is 66 ms, and with our estimated travel time uncertainties, the χ^2 of the model is 1.767.

5. Gravity Modeling

The lack of ray coverage through the continental slope (Figure 14) means we cannot model the thickness of the unextended and weakly extended continental crust from the seismic data; this was not the main target of our experiment. To constrain this portion of the model, the P wave velocity model was converted to density and the gravity anomaly was calculated. The calculated anomaly was compared to the surface gravity anomaly recorded during seismic data acquisition and the model boundaries in the seismically unconstrained region were adjusted to give our final velocity model in such a way as to minimize the misfit between the computed and observed gravity anomalies.

The refraction velocity model has been converted to density using the relationship ρ = -0.6997 + 2.2302V_p - 0.598V_p^2 + 0.07036V_p^3 - 0.0028311V_p^4, with mantle density set at a uniform 3.30 g cm^{-3}. This is a fourth-order polynomial fit (C. A. Zelt, Gravmod user manual, internal document, Cambridge University, 1994) to the relationship of *Ludwig et al.* [1970]. For the sediment layers this function gives a close fit to the marine sediment velocity-density relationship derived from abyssal plain sediments, marine turbidites, and sedimentary rocks of terrigenous source [*Hamilton*, 1977], compatible with what we expect on a rifted continental margin. For the basement density conversion the function closely resembles that for oceanic crustal rocks (V_p >4 km s^{-1}), including serpentinites [*Carlson and Raskin*, 1984; *Miller and Christensen*, 1997] and was therefore considered suitable for the Iberia Abyssal Plain where in region ii the basement composition is undetermined.

The observed gravity anomaly was corrected for drift using land station ties conducted before and after the cruise (<2.5 mGal in 35 days). The resulting shipboard anomaly differs from satellite-derived gravity [*Sandwell and Smith*, 1997] by <5 mGal in general. In calculating the gravity anomaly we assume that the density model does not vary out of the plane of the section. To reduce edge effects, the ends of the model are extended a distance equal to the full width of the original model.

In general, a good correlation is found between calculated and observed gravity (Figure 7b). The distinct broad gravity high observed above the peridotite ridges is duplicated in the calculated anomaly and is explained by the existence of high densities at shallow depth in the basement. The thickness of crust beneath the continental slope was required to be increased to up to 28 km to match the large negative anomaly observed but is not directly constrained by the seismic data. The thickness is dependent on the velocity (density) chosen for the lower crust, but the highest velocity modeled by the seismic data of 6.8 km s^{-1} is close to the average velocity observed in continental crust at 25–30 km depth (6.6–6.9 km s^{-1} [*Christensen and Mooney*, 1995]) and was therefore used as the velocity for the whole of the lower continental crust. Increasing the thickness of the crust to >28 km caused a higher-amplitude negative anomaly to be calculated at a model distance of 295 km. While this improved the fit between the calculated and observed gravity low, it reduced the anomaly over the continental slope to 50 mGal lower than that observed. Our modeled crustal thickness compares with those calculated from wide-angle seismic data acquired on land

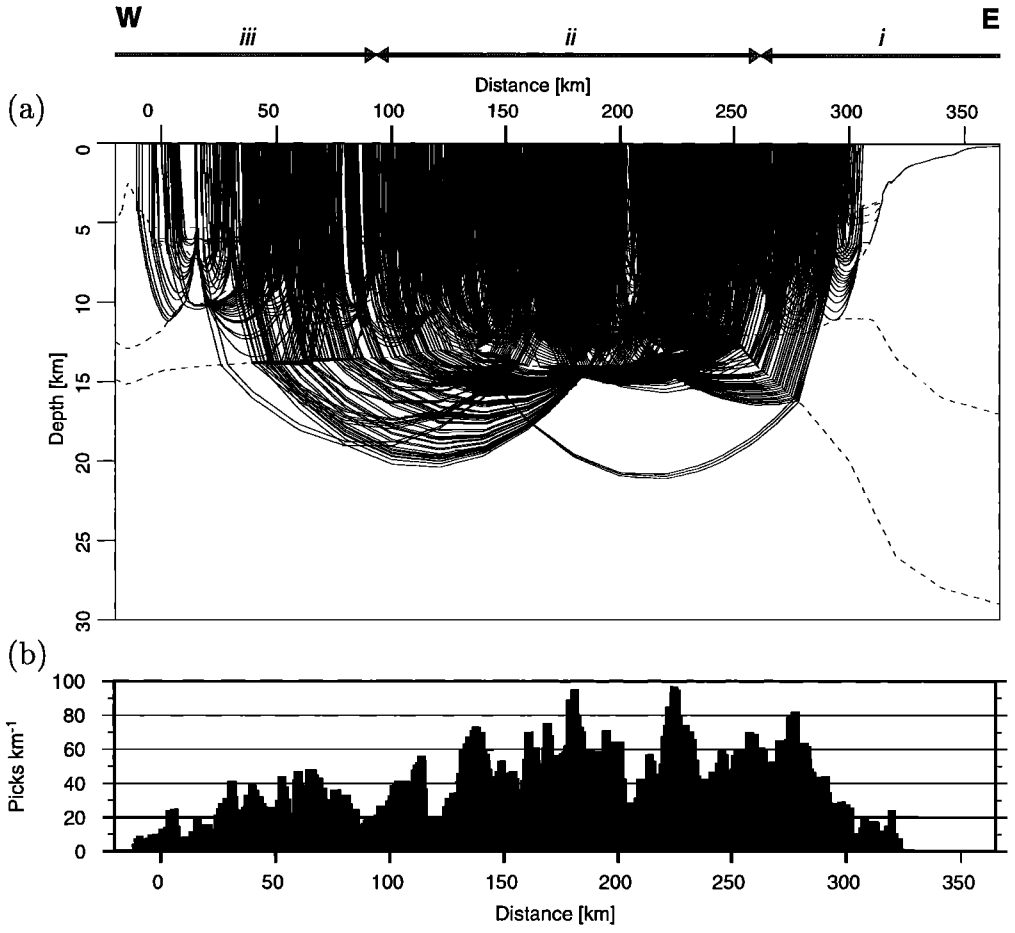

Figure 14. (a) Ray coverage through the model from a total of 10,187 travel time picks (1 ray in 10 plotted) fitted during point-to-point ray tracing with an RMS error of 66 ms. (b) Pick density displayed as the number of picks per 1 km bin along the length of the model, showing the dense ray coverage within the transition zone (region ii).

of 26–27 km (northwest Spain [*Córdoba et al.*, 1988]) and 31 km (near Nazaré [*Moreira et al.*, 1982]). The final RMS misfit of 13 mGal between satellite-derived and calculated gravity anomaly in our model is probably due to off-line structure, particularly beneath the continental slope; the calculated anomaly at the west (oceanward) end of the profile diverges from that observed due to the existence of a seamount, the bulk of which lies out of the plane of the profile.

6. Discussion

Three main hypotheses as to the nature of the basement in the transition zone have been proposed: (1) extended and tectonically disrupted, possibly intruded continental crust [*Whitmarsh et al.*, 1990; *Whitmarsh and Miles*, 1995; *Whitmarsh and Sawyer*, 1996]; (2) ultraslow seafloor spreading oceanic crust [*Whitmarsh and Sawyer*, 1996]; and (3) exhumed and serpentinized upper mantle [*Boillot et al.*, 1995b; *Brun and Beslier*, 1996; *Pickup et al.*, 1996; *Discovery 215 Working Group*, 1998]. In this section we will discuss the relative merits of each with reference to the constraints from our velocity model and other data.

6.1. Thinned Continental Crust Hypothesis

A layer of highly extended continental crust could explain the thin upper basement layer in the transition zone. *Whitmarsh et al.* [1990] show that two velocity profiles located in the transition zone appear similar to the velocity structure of thinned continental crust in the northern Bay of Biscay [*Whitmarsh et al.*, 1986]. They identify a high-velocity (>7 km s^{-1}), lower crustal layer in the southern IAP which they say may be attributed to magmatic underplating. *Pickup et al.* [1996] observe a two-layer reflective character in the transition zone on the IAM-9 reflection profile, with an unreflective upper basement and highly reflective lower layer. Pickup et al. suggest that if the transition zone were continental in origin, the reflective basement layer could be due to magmatic intrusions into thinned continental crust, and the deeper 7.6 km s^{-1} high-velocity layer could be uppermost mantle which has undergone serpentinization with seawater influx through the extended conti-

nental crust. However, *Pickup et al.* [1996] identify a number of distinctive features which are unique to the basement of the transition zone and suggest it is not extended continental crust. Although a reflective layer is observed in the lower continental crust in some areas [*Matthews*, 1986], such a layer is not observed beneath the continental rise along IAM-9 which has an otherwise uniform crustal reflectivity (Figure 3). Thinned continental crust adjacent to the continental rise is observed as a series of fault bounded blocks [*Pickup et al.*, 1996]. The faults dip away from the continent and cause significant basement relief. In contrast, in the transition zone the basement relief is in general subdued [*Discovery 215 Working Group*, 1998]. Intrabasement reflectors which intersect the top of basement do so without any clear offset in the basement surface and those few that cut deep into the section dip predominantly toward the continent.

In our seismic velocity model (Figure 7a) we observe a distinct change in velocity structure at a model distance of 260 km which coincides with the oceanward extent of continental fault blocks. Upper crustal velocities in the transition are the same or lower than that in the adjacent uppermost continental crust. A similar contrast in the velocity at the top of the IAP basement between continental crust and transition zone has been mapped by *Chian et al.* [1999]. The upper crustal velocities are not compatible with thinned continental crust intruded by igneous material which we would expect to increase the seismic velocity.

Lower crustal layers with velocity >7 km s^{-1} are observed on many North Atlantic continental margins and have been interpreted as magmatic material underplating or intruding into continental crust, for example, Hatton Bank and Carolina Trough [*Fowler et al.*, 1989; *Tréhu et al.*, 1989]. In the southern IAP we observe a lower crustal layer with velocity 7.3–7.9 km s^{-1} and a maximum thickness of ~4 km. Melt material underplating thinned continental crust with velocity in excess of 7.2 km s^{-1} would suggest mantle potential temperatures >1500°C at the time of rifting for an unfractionated melt formed by adiabatic decompression melting of the asthenosphere [*White and McKenzie*, 1989]. For such a highly elevated mantle temperature we would expect the oceanic crustal thickness formed directly after rifting to be unusually thick, but this is not observed (Figure 7a). While melt fractionation can lead to the formation of cumulates with a velocity in the region 7.5–7.9 km s^{-1} [*Farnetani et al.*, 1996], these are formed only in plume-related volcanism where huge volumes of melt are generated. The ODP Site 900 gabbro may represent the only significant quantity of synrift magmatic material sampled in the transition zone. The gabbro has a mid-ocean ridge basalt (MORB) origin, with very little, if any contamination by continental crust [*Seifert et al.*, 1996; *Whitmarsh and Sawyer*, 1996]. In the absence of significant synrift volcanism exposed on the thinned continental crust or onshore or the identification of seaward dipping reflectors, it seems unreasonable to attribute the lower crustal layer to magmatic underplating unless we introduce some ad hoc mixing of magmatic and mantle material to increase the velocity [*Whitmarsh et al.*, 1996]. Our wide-angle seismic data are therefore not in agreement with the conclusion that the transition zone is extended and intruded continental crust.

6.2. Slow Spreading/Very Slow Spreading Oceanic Crust Hypothesis

Sawyer [1994] and *Whitmarsh and Sawyer* [1996] present the case for very slow spreading oceanic crust (<10 mm yr^{-1} half rate) in the southern IAP based on basement drilling, crustal thickness, and the age of the oldest recognized seafloor spreading magnetic anomalies. *Sawyer* [1994] estimates a spreading half rate of ~2 mm yr^{-1} for the transitional basement based on sediments sampled at Site 901; *Whitmarsh and Sawyer* [1996] estimate a half rate of ~5 mm yr^{-1}. *Srivastava et al.* [1998] develop the slow spreading oceanic crust hypothesis in the southern IAP by comparison to the crustal velocity structure and magnetic modeling in the central Labrador Sea region, formed at very slow spreading rates.

At very slow spreading rates, more mechanical extension of the crust is thought to occur [*Mutter and Karson*, 1992]. Basement sampling [*Sawyer et al.*, 1994; *ODP Leg 173 Shipboard Scientific Party*, 1998] recovered upper mantle peridotite and serpentinized peridotite over a broad region, which may have been exposed by the extensional faulting of oceanic crust. However, a slow rate of seafloor spreading results in rough basement topography [*Macdonald*, 1982], and with the exception of the peridotite ridges, we observe a low relief basement in the OCT (Figure 3) [*Pickup et al.*, 1996]. The ~0.5 km of basement relief in the OCT does appear to be similar to the basement relief of seismic reflection profiles from slow spreading oceanic crust described by *Mutter and Karson* [1992], but these profiles are taken from an area which is anomalously smooth compared to slow spreading oceanic crust elsewhere, which shows typically >1 km of relief [*Minshull*, 1999]. In addition, basement sampling in the OCT failed to recover any cores of extrusive igneous rock typical of upper oceanic crust.

At ocean ridges where spreading rates fall below 10 mm yr^{-1} half rate a sharp reduction in the thickness of igneous crust formed from mantle melting occurs [*Bown and White*, 1994]. In the southern IAP the thickness of the transitional basement is 3.5–6.0 km (Figure 11a) compared to an average oceanic thickness of 7.1 km away from anomalous regions such as fracture zones and hotspots [*White et al.*, 1992]. However, *Mutter and Mutter* [1993] conclude from a compilation of oceanic crustal structure (ridges and midplate settings) from seismic refraction studies that oceanic

crustal structure is dominated by variations in the thickness of layer 3. Compared to oceanic crust in the North Atlantic [*White et al.*, 1992], the upper, high-velocity-gradient crustal layers (layers B1, B1a, and B2; Figure 7a) lie within the general bounds of oceanic layer 2, but no layer 3 type velocity layer is observed (Figure 11a). Therefore, from the velocity model alone the upper crust within the OCT could be oceanic crust formed at a slow enough spreading rate such that no oceanic layer 3 crust was formed. However, the occurrence of the high-velocity, lower basement layer (layer B3; Figure 7a) and the complete absence of an oceanic layer 3 is unlike that observed at very slow spreading rates, for example the South-West Indian Ridge with a very slow spreading half rate of 8 mm yr^{-1} (Figure 11A) [*Muller et al.*, 1997; *Muller*, 1998].

Very slow spreading oceanic crust was thought to be characterized by weak magnetic anomalies. East of the J anomaly and within the transition zone, magnetic anomalies are generally lower in amplitude than those oceanward [*Whitmarsh and Miles*, 1995]. However, seafloor spreading even at very slow spreading rates, for example, Kolbeinsey Ridge [*Vogt et al.*, 1980] and the South-West Indian Ridge [*Muller et al.*, 1997], can generate linear seafloor spreading magnetic anomalies. A few linear magnetic anomalies, subparallel to the margin are identified in the transition zone, but they do not form continuous linear features [*Whitmarsh and Miles*, 1995; *Discovery 215 Working Group*, 1998], nor have they been successfully modeled at spreading rates <10 mm yr^{-1} [*Whitmarsh and Miles*, 1995]. The magnetic anomalies within the OCT may be attributed to original heterogeneities in the peridotite or to isolated intrusions [*Discovery 215 Working Group*, 1998]; given a roughly east-west extension direction, isolated magmatic intrusions may reasonably be aligned north-south, consistent with the magnetic anomalies.

Sawyer [1994] and *Whitmarsh and Sawyer* [1996] estimate very slow spreading rates under the assumption that (1) Site 901 is the oceanward extent of continental crust (which is no longer valid since Site 1069, 60 km west of Site 901 overlies what is interpreted to be continental crust [*ODP Leg 173 Shipboard Scientific Party*, 1998]); (2) no extension occurred in the crust between Site 901 and the continental shelf; and (3) the shallow marine sediment at Site 901 were deposited at the start of rifting (which cannot be true since Site 901 has subsided to ~3.5 km; see section 6.4 for our determination of the duration of rifting). Therefore we believe it is more appropriate to compare the transitional basement to oceanic crust formed at a spreading half rate faster than 5 mm yr^{-1}.

West of the peridotite ridge, velocity-depth profiles at the instrument locations closely resemble that of Atlantic oceanic crust (Figure 11b). A normal high-velocity-gradient oceanic layer 2 over a normal low-velocity-gradient layer 3 velocity structure is observed [*White et al.*, 1992]. The preexisting wide-angle seismic line 3 located 15 km west of the peridotite ridge was also interpreted in terms of oceanic crust [*Whitmarsh et al.*, 1990]. The velocity model for line 3 is slightly different to our structure for the IAM-9 profile at their intersection, however, with a slightly lower upper crustal velocity of 4.0–5.4 km s^{-1} and higher lower crustal velocity of 7.55–7.7 km s^{-1} (Figure 11b). Since line 3 was shot mainly using widely spaced explosive sources into only two instruments, the structure, especially of the upper crust, is less well constrained. In the same region, M series linear magnetic seafloor spreading anomalies are identified which indicate spreading at a half rate ~10 mm yr^{-1} [*Whitmarsh et al.*, 1990; *Whitmarsh and Miles*, 1995]. Therefore we also interpret the region west of the peridotite ridge as oceanic crust which formed at a slow spreading half rate of ~10 mm yr^{-1}.

In the transition zone, directly east of the peridotite ridge we observe upper basement velocities very similar to those observed west of the peridotite ridge but with the addition of a ~4.5 km s^{-1} layer of low-velocity-gradient at the top of the basement. *Whitmarsh et al.* [1996] model a similar velocity layer at the top of what they interpret as oceanic crust west of the peridotite ridge off Galicia Bank (line 8, Figure 11b). However, closer to the continent the ~4.5 km s^{-1} layer thickens and increases in velocity and the high gradient layer directly below it thins and increases in gradient until a significant velocity step develops. The high-velocity, lower basement layer observed within the OCT (layer B3, Figure 7a) has gradient and thickness similar to the lower crust west of the peridotite ridge but with velocity 0.5–1.0 km s^{-1} higher. Finally, compared to the basement west of the peridotite ridge, the basement in the transition zone has different characteristic features; west of the peridotite ridge the basement relief is higher, and no layered crustal reflectivity is observed [*Pickup et al.*, 1996].

We conclude that though the basement in the transition zone has both an upper crustal velocity structure similar to slow spreading oceanic crust and both types of basement have weak magnetic anomalies, in detail it does not resemble either very slow spreading oceanic crust (<10 mm yr^{-1} half rate) or North Atlantic oceanic crust or the slow spreading oceanic crust west of the peridotite ridges (~10 mm yr^{-1} half rate).

6.3. Exhumed Upper Mantle Hypothesis

That the transition zone consists of exhumed upper mantle material is suggested initially from the wide occurrence of mantle-derived peridotite and serpentinized peridotite in basement samples from the peridotite ridge west of Galicia Bank [*Boillot et al.*, 1980] and from within the transition zone in the southern IAP [*ODP Leg 173 Shipboard Scientific Party*, 1998]. *Pickup et al.* [1996] propose this model for the transition zone in the southern IAP to explain the reflective and unreflective layers in the transitional basement and the

lack of a Moho reflector in the transition zone. In their model the degree of serpentinization varies with the amount of seawater-induced alteration, which decreases with depth into the basement. Vigorous seawater circulation along faults in the uppermost basement, perhaps aided by hydrothermal circulation, resulted in very high degrees of serpentinization and the unreflective top basement observed. In this model the Moho marks a serpentinization front, i.e., the depth to which water was able to percolate down fault planes cutting deep into the upper mantle.

The lower 7.3–7.9 km s^{-1} layer observed across the transition zone is very similar in velocity and thickness to that observed on other nonvolcanic rifted margins (Figure 1), for example, off southwest Greenland [*Chian and Louden*, 1994], southern Labrador [*Chian et al.*, 1995], off Newfoundland [*Reid*, 1994], and Galicia Bank [*Whitmarsh et al.*, 1996]. Serpentinized upper mantle material has been proposed as the best explanation for the high-velocity layer beneath the Iberia Atlantic margin [*Whitmarsh et al.*, 1993; *Boillot et al.*, 1995a; *Brun and Beslier*, 1996; *Pickup et al.*, 1996]. Velocities of >7.3 km s^{-1} are consistent with <25% serpentinization of mantle peridotite [*Miller and Christensen*, 1997]. Since the upper basement is <3 km thick, this serpentinization could have been achieved by hydrothermally driven water influx and possibly aided by circulation along faults [*Pickup et al.*, 1996]. We conclude that this is our favored model for the basement in the southern IAP.

What is less clear with this interpretation is the composition of the upper basement in the transition zone. The velocities observed for the upper basement are within the bounds predicted for peridotite serpentinized between ~25% and 100% [*Miller and Christensen*, 1997], although the range of possible velocities for serpentinized peridotite is very wide and the velocities observed equally lie within the bounds of upper oceanic crust (Figure 11a). Two ODP legs have cored sections of serpentinized basement material up to 140 m thick at three sites (897, 899, and 1068) in the transition zone [*ODP Leg 173 Shipboard Scientific Party*, 1998]. An apparent anomaly is Site 1069, inferred to be underlain by thinned continental crust, which lies west of Site 1068 [*ODP Leg 173 Shipboard Scientific Party*, 1998]. In our profile there has been no basement sampling, but the upper basement velocity is too low to consist of predominantly continental crust.

Bown and White [1995] predict little or no rift related magmatism in the southern IAP. Their calculation assumes a normal asthenospheric mantle temperature of 1300°C, that rifting lasted 25 m.y., that the transition zone is thinned continental crust (based on the interpretation of *Whitmarsh et al.* [1990]), that the high-velocity, lower layer is serpentinized upper mantle, and that β is ~12. If the transition zone contains little or no continental crust, $\beta \rightarrow \infty$, and the amount of decompression melting will increase. In addition, estimates of the age of postrift/prerift sediments from seismostratigraphy and deep drilling in the southern IAP during ODP Leg 149 suggests that the duration of rifting could be as little as 5 m.y. [*Wilson et al.*, 1996]. Such rapid extension would result in a significantly thicker igneous crust than previously predicted by Bown and White. More recent drilling and new modeling of seafloor spreading magnetic anomalies provide the latest constraint on the duration of rifting from which we can calculate bounds for the thickness of rift related igneous material which may have been added to the crust in the southern IAP.

6.4. Duration of Rifting

Different dates for the initiation of seafloor spreading have been recognized for different regions along the West Iberia Atlantic margin consistent with the onset of seafloor spreading from south to north. In the Tagus Abyssal Plain the initiation of seafloor spreading was determined from surface magnetic profiles by *Pinheiro et al.* [1992] and *Whitmarsh and Miles* [1995] to coincide with the M11 anomaly (133 Ma; using the Mesozoic timescale of *Gradstein et al.* [1994]). In the southern IAP, *Whitmarsh et al.* [1990] modeled surface magnetics using a constant spreading rate along a single E-W profile at ~40°30'N. They interpret seafloor spreading to have started somewhere within the first half of anomaly M3 (~126 Ma) at a half rate of between 9.5 and 11 mm yr^{-1} and identify the J magnetic anomaly to have formed just before M0 (121 Ma). Later modeling by *Whitmarsh and Miles* [1995], using nine surface E-W profiles between 40°N and 41°N matched magnetic anomalies back to M8 (129 Ma), but the anomalies prior to M3 were not distinctly observed when a single higher-resolution deep-towed magnetic profile along the ODP Legs 149 and 173 transect was modeled. Here, they identified M3 as the earliest seafloor spreading magnetic anomaly. The latest evaluation of the surface magnetics anomalies along the IAM-9 profile using inverse techniques does not identify magnetic anomalies older then M3 (S. M. Russell, personal communication, 1998). The J magnetic anomaly is not observed off Galicia Bank; oceanic crust here was first formed during the Cretaceous Magnetic Quiet Interval (post-120 Ma), later than in the southern IAP [*Ogg*, 1988; *Pinheiro et al.*, 1996]. Therefore, from the seafloor spreading magnetic anomalies the rifting event which opened the North Atlantic propagated from south to north. The best constraint on the initiation of seafloor spreading in the southern IAP is that it occurred close to 126 Ma.

The Ocean Drilling Program has sampled prerift to synrift (early Tithonian, ~149 Ma) shallow marine sediments at Site 901 [*Sawyer et al.*, 1994] and similar, but thinner sediment units at Sites 1065 and 1069 [*ODP Leg 173 Shipboard Scientific Party*, 1998]. At Site 1069 this unit is overlain by a slumped chalk of upper Berriasian–lower Valanginian age [*ODP Leg 173 Shipboard Scien-*

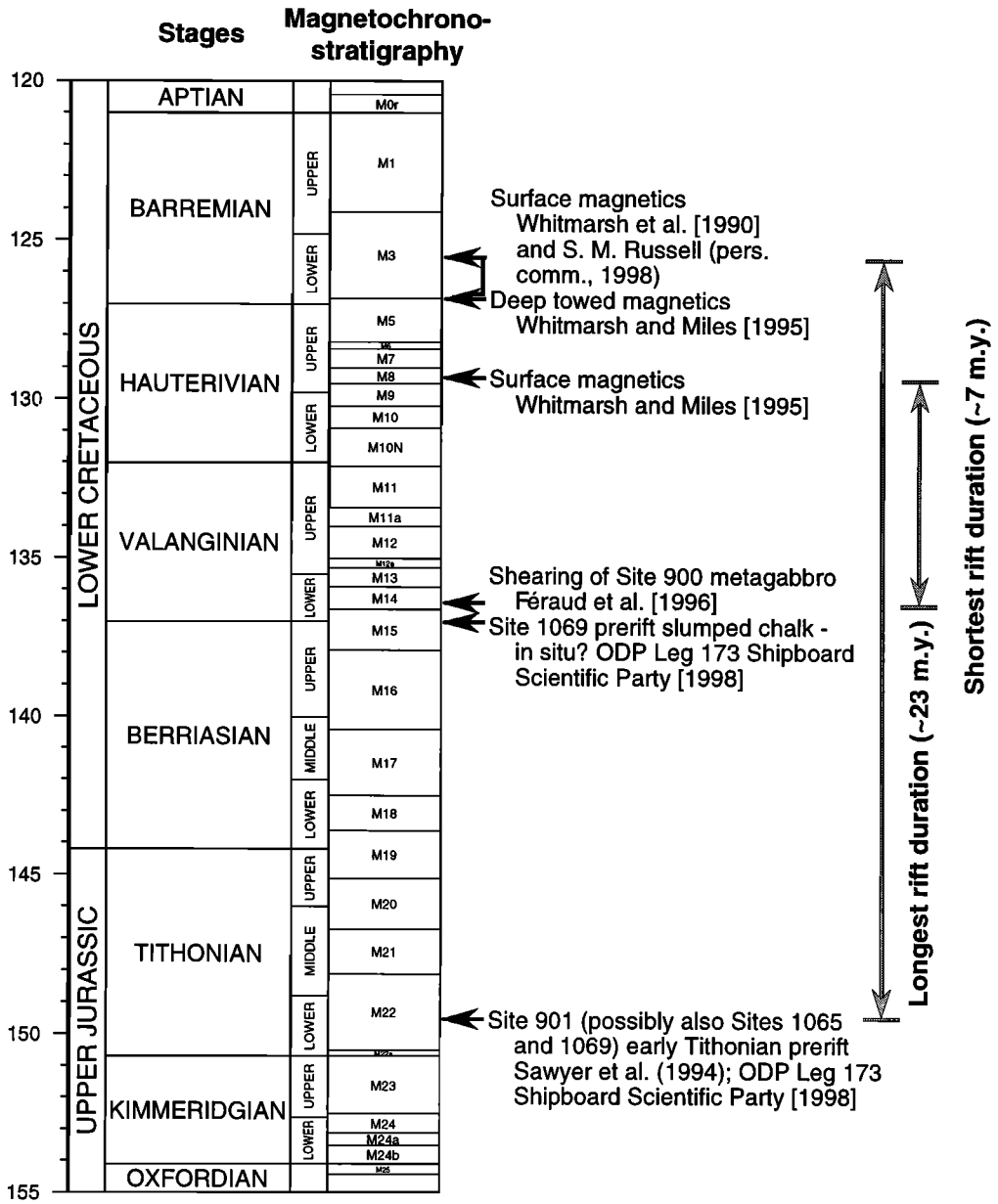

Figure 15. Summary of evidence regarding the timing and duration of rifting in the southern Iberia Abyssal Plain (modified from *Wilson et al.* [1996]). Magnetic anomalies indicate the initiation of seafloor spreading. The duration of the rifting episode which led to seafloor spreading is determined to be between 7 and ~23 m.y. The timescale used is that of *Gradstein et al.* [1994].

tific Party, 1998]. *Wilson et al.* [1996] suggest rifting in the southern IAP occurred during the latest Berriasian and earliest Valanginian, but this is based on the results of drilling over Galicia Bank (Leg 103) and the assumption that rifting occurred in both areas simultaneously. The upper Berriasian–lower Valanginian chalk at Site 1069 formed in a shallow marine environment [*ODP Leg 173 Shipboard Scientific Party*, 1998], but it is not in situ and could be sourced from the Galicia Bank high after rifting started in the southern IAP. Plagioclase in sheared metagabbro at Site 900, interpreted as a synrift melt product, was dated by $^{40}Ar/^{39}Ar$ at 136.4±0.3 Ma by *Féraud et al.* [1996]. The initiation of rifting must predate the shearing of the Site 900 gabbro but postdate the Site 901, Site 1065, and Site 1069 Tithonian sediments. The northward propagation of rifting may mean that rifting occurred earlier on the IAM-9 profile than at the Ocean Drilling Program transect. However, the distance between the two profiles is small (~40 km), so we do not expect the difference to be large.

We place the bounds for the duration of rifting (including formation of the transition zone) at an absolute minimum of (136.4–129) ~7 m.y., which is in close agreement with that of *Wilson et al.* [1996]. However,

with the current lack of dated, in situ prerift sediments younger than the early Tithonian and considering that seafloor spreading more likely started within the M3 polarity interval, the duration of rifting could be as long as (149–126) 23 m.y. The dating constraints are summarized in Figure 15.

6.5. Decompression Melt in an Exhumed Upper Mantle

From our velocity model (Figure 7a) we calculate a hypothetical maximum melt thickness of ~4.5 km in the transition zone. This thickness is based under the assumption that (1) The 7.3–7.9 km s^{-1} layer does contain some melt (from the velocity and average thickness of ~4 km, we estimate a maximum of ~1.5 km could be added to the thickness of igneous crust by some ad hoc mixing of magmatic and mantle material distributed throughout the layer, and not accumulated into regions which can be seismically resolved); (2) the upper, high-velocity-gradient crustal layers (layers B1, B1a, and B2; Figure 7a), which are on average ~3 km thick, are formed entirely from melt products. However, the melt thickness in the transition zone is probably much less than 4.5 km. We believe that the 7.3–7.9 km s^{-1} layer does not contain any melt (see above) and that the upper, high-velocity-gradient crustal layers cannot be formed entirely from melt products since basement sampling recovered mostly upper mantle peridotite and serpentinized peridotite within this region, and no strong magnetic anomalies are observed. A small melt thickness is consistent with the light rare earth element enriched mafic igneous rocks recovered at ODP Sites 899 and 900 [*Seifert et al.*, 1997] which indicates low degrees of melting [*Discovery 215 Working Group*, 1998].

Using our estimated bounds of 7–23 m.y. for the duration of rifting and β=15, the maximum value for which *Bown and White* [1995] model the Iberia Atlantic margin, we estimate that the basement should contain a minimum thickness of between 1 and 3.5 km of igneous material from mantle melting [*Bown and White*, 1995, Figure 13]. For β=50 the melt thickness rises to between 3 and 5 km [*Whitmarsh et al.*, 1996], and presumably, at even higher β factors the melt thickness will increase further.

The above argument for melting assumes that a pure shear mechanism has dominated rifting. Simple shear deformation significantly reduces the degree of melting which occurs from mantle upwelling. *Latin and White* [1990] calculate that for an asthenospheric mantle temperature of 1280°C, simple shear along a planar detachment does not cause any decompression melting even beyond β=50. Simple shear deformation models have been proposed for the West Iberia Atlantic margin, predominantly to explain the low-angle reflection event "S" identified west of Galicia Bank [e.g., *Boillot et al.*, 1995a; *Krawczyk and Reston*, 1995]. A difficulty with models involving simple shear throughout the evolution of the margin is that a gross asymmetry with the conjugate margin is predicted. Wide-angle seismic models for South Flemish Cap [*Todd and Reid*, 1989] and the southern Newfoundland margin [*Reid*, 1994], which are the nearest to conjugate, appear rather similar to our model for the southern IAP. Also, there are no crustal scale low-angle reflectors observed beneath continental crust in the IAM-9 profile. Therefore, while simple shear processes cannot be excluded in the final stages of breakup, we see no evidence for large-scale, i.e., lithospheric, simple shear at 40°20'N on the Iberia Atlantic margin.

Since we see no evidence for the predicted voluminous quantities of melt, either the effective β factor is <50 or the model for melting does not work for very high β factors. We conclude that there is either no melt present in the transition zone or $\ll$4.5 km of melt is distributed in some way that drilling has failed to sample it. Owing to the depth involved, basement sampling in the transition zone has been limited to the topographic highs spaced at ~20-km intervals. The distribution of melt material in the basement may be such that either it is below or within a layer of mainly serpentinized peridotite (vertically heterogeneous) and/or is not uniformly distributed across the region (laterally heterogeneous).

The presence of serpentinized peridotite above melt material in the transition zone upper basement could result from two mechanisms. A thin igneous crust formed during slow extension would be heavily faulted, allowing seawater influx and serpentinization of the underlying mantle [*Escartín et al.*, 1997]. The serpentinization of peridotite causes a reduction in density [*Miller and Christensen*, 1997]; any highly serpentinized material is therefore buoyant relative to peridotite and may migrate upward along fault planes, so that some is now found above the igneous crust [*Francis*, 1981]. However, we would expect the igneous layer to produce recognizable magnetic anomalies. An alternative mechanism is that the basement is formed by the serpentinization of exposed mantle peridotite which is then subsequently intruded by the products of decompression melting of underlying, unserpentinized mantle peridotite. The density of peridotite is linearly related to the degree of serpentinization, lying in the range 2.5–3.3 Mg m^{-3} [*Miller and Christensen*, 1997]. The velocity of the top basement in the transition zone is slightly less than the velocity of peridotite serpentinized 100%. We suggest that this is due to the highly faulted nature of the basement and brecciation of the uppermost layer. Basaltic melts have a mean density of 2.7 Mg m^{-3} [*Hooft and Detrick*, 1993]. Although the density is dependent on the degree of fractionation, 2.7 Mg m^{-3} represents a theoretical minimum density [*Hooft and Detrick*, 1993, Figure 2] and corresponds to a P wave velocity of ~6 km s^{-1} in serpentinized peridotite [*Miller and Christensen*, 1997, Figures 8 and 9]. Therefore melt would pond in a highly serpentinized basement due to buoyancy [e.g., *White and McKenzie*, 1989] at a depth of 1–2 km in our velocity model (Figures 11 and 7).

This model assumes that significant volumes of serpentinized peridotite are not taken above the 500°C stability limit [*Toft et al.*, 1990] when intruded by melt and may not be valid if the thickness of melt intruded is large. The top of the reflective layer in IAM-9 occurs 0.5–1.0 s (1–2 km) below the top of the basement, and this layer may be 0.5 s (1 km) thick (Figures 3 and 4). The depth of this layer roughly coincides with basement layer B2 in the transition zone and is consistent with the subbasement magnetic source depths constrained by a two-dimensional Euler deconvolution of the magnetic anomalies along the IAM-9 profile [*Discovery 215 Working Group*, 1998].

A laterally variable distribution of igneous material could be the result of melting which is not focused at a single spreading center but is distributed over a diffuse region of extending crust. At mid-ocean ridges, melt is focused from a broad region of partial melt to a narrow spreading center [*MELT Seismic Team*, 1998]. However, in areas of continental rifting, crustal extension (and presumably melt intrusion and underplating) is commonly distributed over a wide region [e.g., *England and Jackson*, 1989]. Continental breakup followed by seafloor spreading must involve a transition between these two modes of deformation and melt supply. An unfocused melt accumulation in the crust is consistent with the paucity of linear magnetic anomalies in the transition zone [*Whitmarsh and Miles*, 1995; *Discovery 215 Working Group*, 1998]. Although the velocity structure along IAM-9 does not show strong lateral variations, except at the peridotite ridges, the length scale of the variations could be below the seismic resolution.

7. Conclusion

Wide-angle seismic data from 13 ocean bottom instruments at 40°20'N in the southern Iberia Abyssal Plain passive continental margin have been modeled and interpreted together with seismic reflection, gravity, magnetics and Ocean Drilling Program information to constrain crustal structure and composition within the ocean-continent transition.

1. The velocity structure along our refraction profile allows four distinct zones to be described. These are, from west to east, oceanic crust, peridotite ridge overlap, transition zone, and thinned continental crust.

2. Oceanward of the peridotite ridge, we observe oceanic crust of 6.5–7 km thickness, 0.5-1.0 km thinner than normal for Atlantic oceanic crust aged 59–170 Ma, and an otherwise normal oceanic layer 2/layer 3 velocity structure. The location and nature of the transition from peridotite ridge to oceanic crust in the velocity model are poorly constrained, but the data do not support any sharp lateral variation in the upper crustal velocities similar to that observed on the continental flank.

3. Continental crust is defined by velocities in the range 5.5–6.8 km s^{-1}, rotated crustal blocks bounded by faults, and a Moho reflection on the coincident seismic reflection profile. Across the lower continental slope and rise, the crust thins from 28 to 7 km over a distance of 80 km. A large and abrupt (1 km s^{-1} in <5 km) lateral reduction in upper crustal velocity and a decrease in basement relief coincide with the boundary from the most oceanward continental fault block into the basement of the transition zone.

4. The ocean-continent transition along our profile includes two apparently overlapping segments of a peridotite ridge identified from basement topographic highs and direct sampling. In the velocity model the ridges are observed as a single 50-km-wide region distinguished from the rest of the transition zone by a reduced top basement velocity and by elevated middle crust velocities. The raised basement relief and velocity structure coincide with the reflector L2 on the landward flank of the region, one of a pair of prominent deep reflection events observed below the peridotite ridges.

5. A 170-km-wide transition zone including a pair of overlapping peridotite ridges is characterized by a velocity structure which does not resemble either continental or oceanic crust. An upper, high-velocity-gradient layer 2–4 km thick is interpreted to be upper mantle peridotite serpentinized between 25% and 100%, which may have subsequently been intruded locally by the products of decompression melting in the mantle. Serpentinization has occurred by seawater influx during rifting along a large numbers of faults which have brecciated the top 1 km. A lower layer up to 4 km thick with velocity of 7.3–7.9 km s^{-1} represents mantle peridotite with mean bulk serpentinization of <25%, possibly concentrated along fewer, but deep cutting fault planes. This layer can contain only a few percent, if any, melt material. The Moho in the southern IAP consists of a gradual transition from serpentinized upper mantle peridotite to unserpentinized peridotite with velocity 8 km s^{-1}; hence only weak, wide-angle Moho reflections are observed and normal-incidence reflections are absent.

6. While it is likely that there are some melt products in the transition zone, our results suggest that the thickness is much less than the 3–5 km predicted by *Bown and White*'s [1995] model for β=50 and an estimated rift duration of 7–23 m.y.

Acknowledgments. This work was supported by grants from the United Kingdom Natural Environment Research Council (grant GR3/9354 to T.A.M. and R.B.W.) and the Natural Sciences and Engineering Research Council of Canada (grant CSPO149903 to K.E.L.). S.M.D. was supported by a Natural Environment Research Council Studentship. T.A.M. was supported by a Royal Society University Research Fellowship. Department of Earth Sciences, University of Cambridge, contribution 5553.

References

Banda, E., M. Torné, and Iberia Atlantic Margins Group, Iberia Atlantic Margins Group investigates deep structure of ocean basins, *Eos Trans. AGU, 76*, 25–29, 1995.

Beslier, M.-O., M. Ask, and G. Boillot, Ocean-continent boundary in the Iberia Abyssal Plain from multichannel seismic data, *Tectonophysics, 218*, 383–393, 1993.

Boillot, G., S. Grimaud, A. Mauffret, D. Mougenot, J. Kornprobst, J. Mergoil-Daniel, and G. Torrent, Ocean-continent boundary off the Iberian margin: A serpentinite diapir west of the Galicia Bank, *Earth Planet. Sci. Lett., 48*, 23–34, 1980.

Boillot, G., M.-O. Beslier, and J. Girardeau, Nature, structure and evolution of the ocean-continent boundary: The lesson of the west Galicia margin (Spain), in *Rifted Ocean-Continent Boundaries, NATO-Workshop 1994*, edited by E. Banda, M. Torné, and M. Talwani, pp. 219–229, Kluwer, Dordrecht, Netherlands, 1995a.

Boillot, G., M.-O. Beslier, C. M. Krawczyk, D. Rappin, and T. J. Reston, The formation of passive margins: Constraints from the crustal structure and segmentation of the deep Galicia margin, Spain, in *The Tectonics, Sedimentation and Palaeoceanography of the North Atlantic Region*, edited by R. A. Scrutton et al., *Geol. Soc. Spec. Publ., 90*, 71–91, 1995b.

Bown, J. W., and R. S. White, Variation with spreading rate of oceanic crustal thickness and geochemistry, *Earth Planet. Sci. Lett., 121*, 435–449, 1994.

Bown, J. W., and R. S. White, The effect of finite extension rate on melt generation at continental rifts, *J. Geophys. Res., 100*, 18,011–18,030, 1995.

British Oceanographic Data Centre, *GEBCO Digital Atlas*, Birkenhead, United Kingdom, 1997.

Brun, J. P., and M.-O. Beslier, Mantle exhumation at passive margins, *Earth Planet. Sci. Lett., 142*, 161–173, 1996.

Carlson, R. L., and G. S. Raskin, Density of the ocean crust, *Nature, 311*, 555–558, 1984.

Chian, D., and K. E. Louden, The continent-ocean crustal transition across the southwest Greenland margin, *J. Geophys. Res., 99*, 9117–9135, 1994.

Chian, D., K. E. Louden, and I. Reid, Crustal structure of the Labrador Sea conjugate margin and implications for the formation of nonvolcanic rifted margins, *J. Geophys. Res., 100*, 24239–24253, 1995.

Chian, D., K. E. Louden, T. A. Minshull, and R. B. Whitmarsh, Deep structure of the ocean-continent transition in the southern Iberia Abyssal Plain from seismic refraction profiles: The Ocean Drilling Program (Legs 149 and 173) transect, *J. Geophys. Res., 104*, 7443–7462, 1999.

Christensen, N. I., and W. D. Mooney, Seismic velocity structure and composition of the continental crust: A global view, *J. Geophys. Res., 100*, 9761–9788, 1995.

Córdoba, D., E. Banda, and J. Ansorge, *P* wave velocity-depth distribution in the Hercynian crust of northwest Spain, *Phys. Earth Planet. Inter., 51*, 235–248, 1988.

Detrick, R. S., R. S. White, and G. M. Purdy, Crustal structure of North Atlantic fracture zones, *Rev. Geophys., 31*, 439–458, 1993.

Discovery 215 Working Group, Deep structure in the vicinity of the ocean-continent transition zone under the southern Iberia Abyssal Plain, *Geology, 26*, 743–746, 1998.

Dyment, J., J. Arkani-Hamed, and A. Ghods, Contribution of serpentinized ultramafics to marine magnetic anomalies at slow and intermediate spreading centers: Insights from the shape of the anomalies, *Geophys. J. Int., 129*, 691–701, 1997.

Eldholm, O., et al., *Proc. Ocean Drilling Program, Initial Reports*, vol 104, 783 pp., Ocean Drill. Program, College Station, Tex., 1987.

England, P., and J. Jackson, Active deformation of the continents, *Annu. Rev. Earth Planet. Sci., 17*, 197–226, 1989.

Escartín, J., G. Hirth, and B. Evans, Effects of serpentinization on the lithospheric strength and the style of normal faulting at slow-spreading ridges, *Earth Planet. Sci. Lett., 151*, 181–189, 1997.

Farnetani, C. G., M. A. Richards, and M. S. Ghiorso, Petrological models of magma evolution and deep crustal structure beneath hotspots and flood basalt provinces, *Earth Planet. Sci. Lett., 143*, 81–94, 1996.

Féraud, G., M.-O. Beslier, and G. Cornen, $^{40}Ar/^{39}Ar$ dating of gabbros from the ocean-continent transition of the western Iberia margin: Preliminary results, *Proc. Ocean Drill. Program Sci. Results, 149*, 489–495, 1996.

Fowler, S. R., R. S. White, G. D. Spence, and G. K. Westbrook, The Hatton Bank continental margin, II, Deep structure from two-ship expanding spread seismic profiles, *Geophys. J., 96*, 295–309, 1989.

Francis, T. J. G., Serpentinization faults and their role in the tectonics of slow spreading ridges, *J. Geophys. Res., 86*, 11,616–11,622, 1981.

Gradstein, F. M., F. P. Agterberg, J. G. Ogg, J. Hardenbol, P. van Veen, J. Thierry, and Z. Huang, A Mesozoic time scale, *J. Geophys. Res., 99*, 24,051–24,074, 1994.

Hamilton, E. L., Sound velocity-density relations in seafloor sediments and rocks, *J. Acoust. Soc. Am., 63*, 366–377, 1977.

Harry, D. L., and M. Batzle, In situ velocities of sedimentary rocks from the Iberia Abyssal Plain, *Proc. Ocean Drill. Program Sci. Results, 149*, 343–351, 1996.

Hoffmann, H.-J., and T. J. Reston, Nature of the S reflector beneath the Galicia Banks rifted margin: Preliminary results from prestack depth migration, *Geology, 20*, 1091–1094, 1992.

Hooft, E. E., and R. S. Detrick, The role of density in the accumulation of basaltic melts at mid-ocean ridges, *Geophys. Res. Lett., 20*, 423–426, 1993.

Hopper, J. R., and W. R. Buck, The effect of lower crustal flow on continental extension and passive margin formation, *J. Geophys. Res., 101*, 20,175–20,194, 1996.

Horsefield, S. J., R. B. Whitmarsh, R. S. White, and J.-C. Sibuet, Crustal structure of the Goban Spur rifted continental margin, NE Atlantic, *Geophys. J. Int., 119*, 1–19, 1993.

Keen, C. E., and B. de Voogd, The continent-ocean boundary at the rifted margin off eastern Canada: New results from deep seismic reflection studies, *Tectonics, 7*, 107–124, 1988.

Krawczyk, C. M., and T. J. Reston, Detachment faulting and continental breakup: The S reflector offshore Galicia, in *Rifted Ocean-Continent Boundaries, NATO-Workshop 1994*, edited by E. Banda, M. Torné, and M. Talwani, pp. 231–246, Kluwer, Dordrecht, Netherlands, 1995.

Krawczyk, C. M., T. J. Reston, M.-O. Beslier, and G. Boillot, Evidence for detachment tectonics on the Iberia Abyssal Plain rifted margin, *Proc. Ocean Drill. Program Sci. Results, 149*, 603–615, 1996.

Latin, D., and N. White, Generating melt during lithospheric extension: Pure shear vs. simple shear, *Geology, 18*, 327–331, 1990.

Le Pichon, X., and F. Barbier, Passive margin formation by low-angle faulting within the upper crust: The Northern Bay of Biscay margin, *Tectonics, 6*, 133–150, 1987.

Louden, K. E., J.-C. Sibuet, and F. Harmegnies, Variations in heat flow across the ocean-continent transition in the Iberia Abyssal Plain, *Earth Planet. Sci. Lett., 151*, 233–254, 1997.

Ludwig, W. J., J. E. Nafe, and C. L. Drake, Seismic Refraction, in *The Sea*, vol. 4, edited by A. E. Maxwell, pp. 53–84, Wiley-Interscience, 1970.

Macdonald, K. C., Mid-ocean ridges: Fine scale tecton-

ics, volcanic and hydrothermal processes within the plate boundary zone, *Annu. Rev. Earth Planet. Sci., 10*, 155–190, 1982.

Matthews, D. H., Seismic reflections from the lower crust around Britain, in *The Nature of the Lower Continental Crust*, edited by J. B. Dawson et al., *Geol. Soc. Spec. Publ., 24*, 11–22, 1986.

Mauffret, A., D. Mougenot, P. R. Miles, and J. A. Malod, Cenozoic deformation and Mesozoic abandoned spreading centre in the Tagus Abyssal Plain (west of Portugal): Results of a multichannel seismic survey, *Can. J. Earth Sci., 26*, 1101–1123, 1989.

MELT Seismic Team, Imaging the deep seismic structure beneath a mid-ocean ridge: The MELT experiment, *Science, 280*, 1215–1218, 1998.

Miller, D. J., and N. I. Christensen, Seismic velocities of lower crustal and upper mantle rocks from the slow-spreading Mid-Atlantic Ridge, south of the Kane Transform (MARK), *Proc. Ocean Drill. Program Sci. Results, 153*, 437–454, 1997.

Minshull, T. A., On the roughness of Mesozoic oceanic crust in the western North Atlantic, *Geophys. J. Int., 136*, 286–290, 1999.

Moreira, V. S., C. Prodehl, St. Mueller, and A. S. Mendes, Crustal structure of western Portugal, in *Proceedings of the 17th General Association European Seismology Committee, 1980*, pp. 529–532, Budapest, 1982.

Muller, M. R., Crustal structure of the Southwest Indian ridge, Ph.D. dissertation, 242 pp., Univ. of Cambridge, Cambridge, England, 1998.

Muller, M. R., C. J. Robinson, T. A. Minshull, R. S. White, and M. J. Bickle, Thin crust beneath Ocean Drilling Program borehole 735B at the Southwest Indian ridge, *Earth Planet. Sci. Lett., 148*, 93–107, 1997.

Mutter, C. Z., and J. C. Mutter, Variations in thickness of layer 3 dominate oceanic crustal structure, *Earth Planet. Sci. Lett., 117*, 295–317, 1993.

Mutter, J. C., Margins declassified, *Nature, 364*, 393–394, 1993.

Mutter, J. C., and J. A. Karson, Structural processes at slow-spreading ridges, *Science, 257*, 627–634, 1992.

National Geophysical Data Center, ETOP0 5 Bathymetry/topography data, *Data Announcement 88-MGG-02*, Nat. Oceanogr. and Atmos. Admin., U.S. Dep. of Commer., Boulder Colo., 1988.

ODP Leg 173 Shipboard Scientific Party, Drilling reveals transition from continental breakup to early magmatic crust, *Eos Trans. AGU, 79*, 173–181, 1998.

Ogg, J. G., Early Cretaceous and Tithonian magnetostratigraphy of the Galicia margin, *Proc. Ocean Drill. Program Sci. Results, 103*, 659–682, 1988.

Osler, J. C., and K. E. Louden, Extinct spreading center in the Labrador Sea: Crustal structure from a two-dimensional seismic refraction velocity model, *J. Geophys. Res., 100*, 2261–2278, 1995.

Pickup, S. L. B., R. B. Whitmarsh, C. M. R. Fowler, and T. J. Reston, Insight into the nature of the ocean-continent transition off West Iberia from a deep multichannel seismic reflection profile, *Geology, 24*, 1079–1082, 1996.

Pinheiro, L. M., R. B. Whitmarsh, and P. R. Miles, The ocean-continent boundary off the western continental margin of Iberia, II, Crustal structure in the Tagus Abyssal Plain, *Geophys. J. Int., 109*, 106–124, 1992.

Pinheiro, L. M., R. C. L. Wilson, R. Pena dos Reis, R. B. Whitmarsh, and A. Ribeiro, The western Iberia margin: A geophysical and geological overview, *Proc. Ocean Drill. Program Sci. Results, 149*, 3–23, 1996.

Rabinowitz, P. D., S. C. Cande, and D. E. Hayes, The J-anomaly in the central North Atlantic Ocean, *Initial Rep. Deep Sea Drill. Project, 43*, 879–885, 1979.

Reid, I. D., Crustal structure of a nonvolcanic rifted margin east of Newfoundland, *J. Geophys. Res., 99*, 15,161–15,180, 1994.

Sandwell, D. T., and W. H. F. Smith, Marine gravity anomaly from Geosat and ERS-1 satellite altimetry, *J. Geophys. Res., 102*, 803–827, 1997.

Sawyer, D. S., The case for slow-spreading oceanic crust landward of the peridotite ridge in the Iberia Abyssal Plain, *Eos Trans. AGU, 75*(44), Fall Meet. Suppl., 616, 1994.

Sawyer, D. S., et al., *Proceedings of the Ocean Drilling Program, Initial Reports, 149*, 719 pp., Ocean Drill. Program, College Station, Tex., 1994.

Seifert, K., I. Gibson, D. Weis, and D. Brunotte, Geochemistry of metamorphosed cumulate gabbros from Hole 900A, Iberia Abyssal Plain, *Proc. Ocean Drill. Program Sci. Results, 149*, 471–488, 1996.

Seifert, K. E., C.-W. Chang, and D. A. Brunotte, Evidence from Ocean Drilling Program Leg 149 mafic igneous rocks for oceanic crust in the Iberia Abyssal Plain ocean-continent transition zone, *J. Geophys. Res., 102*, 7915–7928, 1997.

Sibuet, J.-C., Formation of non-volcanic passive margins: A composite model applies to the conjugate Galicia and southeastern Flemish Cap margins, *Geophys. Res. Lett., 19*, 769–772, 1992.

Sibuet, J.-C., et al., *Initial Reports of the Deep Sea Drilling Project*, vol. 47, part 2, 787 pp., U.S. Govt. Print. Off., Washington D.C., 1979.

Sibuet, J.-C., V. Louvel, R. B. Whitmarsh, R. S. White, S. J. Horsefield, B. Sichler, P. Léon, and M. Recq, Constraints on rifting processes from refraction and deep-tow magnetic data: The example of the Galicia continental margin (West Iberia), in *Rifted Ocean-Continent Boundaries, NATO-Workshop 1994*, edited by E. Banda, M. Torné, and M. Talwani, pp. 197–217, Kluwer, Dordrecht, Netherlands, 1995.

Srivastava, S. P., J.-C. Sibuet, and S. Cande, Origin of thin crust across the Iberia and Newfoundland passive continental margins: A result of ultraslow seafloor spreading, *Eos Trans. AGU, 79*(45), Fall Meet. Suppl., 854, 1998.

Todd, B. J., and I. Reid, The continent-ocean boundary south of Flemish Cap: Constraints from seismic refraction and gravity, *Can. J. Earth Sci., 26*, 1392–1407, 1989.

Toft, P. B., J. Arkani-Hamed, and S. E. Haggerty, The effect of serpentinization on density and magnetic susceptibility: A petrophysical model, *Phys. Earth Planet. Inter., 65*, 137–157, 1990.

Torné, M., M. Fernandez, J. Carbonell, and E. Banda, Lithospheric transition from continental to oceanic in the West Iberia Atlantic margin, in *Rifted Ocean-Continent Boundaries, NATO-Workshop 1994*, edited by E. Banda, M. Torné, and M. Talwani, pp. 247–263, Kluwer, Dordrecht, Netherlands, 1995.

Tréhu, A. M., A. Ballard, L. M. Dorman, J. F. Gettrust, K. D. Klitgord, and A. Schreiner, Structure of the lower crust beneath the Carolina Trough, U.S. Atlantic continental margin, *J. Geophys. Res., 94*, 10,585–10,600, 1989.

Vogt, P. R., G. L. Johnson, and L. Kristjansson, Morphology and magnetic anomalies north of Iceland, *J. Geophys., 47*, 67–80, 1980.

White, R. S., and D. P. McKenzie, Magmatism at rift zones: The generation of volcanic continental margins and flood basalts, *J. Geophys. Res., 94*, 7685–7729, 1989.

White, R. S., D. P. McKenzie, and R. K. O'Nions, Oceanic crustal thickness from seismic measurements and rare

earth element inversions, *J. Geophys. Res., 97*, 19,683–19,715, 1992.

Whitmarsh, R. B., and P. R. Miles, Models of the development of the West Iberia rifted continental margin at 40°30'N deduced from surface and deep-tow magnetic anomalies, *J. Geophys. Res., 100*, 3789–3806, 1995.

Whitmarsh, R. B., and D. S. Sawyer, The ocean/continent transition beneath the Iberia Abyssal Plain and continental-rifting to seafloor-spreading processes, *Proc. Ocean Drill. Program Sci. Results, 149*, 713–733, 1996.

Whitmarsh, R. B., F. Avedik, and M. R. Saunders, The seismic structure of thinned continental crust in the northern Bay of Biscay, *Geophys. J. R. Astron. Soc., 86*, 589–602, 1986.

Whitmarsh, R. B., P. R. Miles, and A. Mauffret, The ocean-continent boundary off the western continental margin of Iberia, I, Crustal structure at 40°30'N, *Geophys. J. Int., 103*, 509–531, 1990.

Whitmarsh, R. B., L. M. Pinheiro, P. R. Miles, M. Recq, and J.-C. Sibuet, Thin crust at the western Iberia ocean-continent transition and ophiolites, *Tectonics, 12*, 1230–1239, 1993.

Whitmarsh, R. B., R. S. White, S. J. Horsefield, J.-C. Sibuet, M. Recq, and V. Louvel, The ocean-continent boundary off the western continental margin of Iberia: Crustal structure west of Galicia Bank, *J. Geophys. Res., 101*, 28,291–28,314, 1996.

Wilson, R. C. L., D. S. Sawyer, R. B. Whitmarsh, J. Zerong, and J. Carbonell, Seismic stratigraphy and tectonic history of the Iberia Abyssal Plain, *Proc. Ocean Drill. Program Sci. Results, 149*, 617–633, 1996.

Zelt, C. A., and D. A. Forsyth, Modeling wide-angle seismic data for crustal structure: Southeastern Grenville Province, *J. Geophys. Res., 99*, 11,687–11,704, 1994.

Zelt, C. A., and R. B. Smith, Seismic travel-time inversion for 2-D crustal velocity structure, *Geophys. J. Int., 108*, 16–34, 1992.

S. M. Dean and T. A. Minshull, School of Ocean and Earth Sciences, Southampton Oceanography Centre, Southampton SO14 3ZH, England, U.K. (Simon.M.Dean@soc.soton.ac.uk)

K. E. Louden, Department of Oceanography, Dalhousie University, Halifax, Nova Scotia B3H 4J1, Canada. (klouden@is.dal.ca)

R. B. Whitmarsh, Challenger Division, Southampton Oceanography Centre, Southampton SO14 3ZH, England, U.K. (Bob.Whitmarsh@soc.soton.ac.uk)

(Received November 30, 1998; revised July 13, 1999; accepted August 26, 1999.)